AGU PUBLICATIONS

Journal of Advances in Modeling Earth Systems

RESEARCH ARTICLE
10.1002/2016MS000740

**Key Points:**
- The sensitivity of low clouds to shallow convective mixing depends on turbulence and radiation
- The coupling between low-cloud radiative cooling and surface latent heat flux strengthens the low-cloud feedback
- By affecting the relative importance of key processes, the closure of shallow convection schemes affects the strength of low-cloud feedback

**Correspondence to:**
J. Vial,
jessica.vial@lmd.jussieu.fr

**Citation:**
Vial, J., S. Bony, J.-L. Dufresne, and R. Roehrig (2016), Coupling between lower-tropospheric convective mixing and low-level clouds: Physical mechanisms and dependence on convection scheme, *J. Adv. Model. Earth Syst.*, *8*, 1892–1911, doi:10.1002/2016MS000740.

Received 21 JUN 2016
Accepted 3 NOV 2016
Accepted article online 12 NOV 2016
Published online 9 DEC 2016



# Coupling between lower-tropospheric convective mixing and low-level clouds: Physical mechanisms and dependence on convection scheme

**Jessica Vial[1], Sandrine Bony[1], Jean-Louis Dufresne[1], and Romain Roehrig[2]**

[1]Laboratoire de Météorologie Dynamique, Université Pierre et Marie Curie (UPMC), Paris, France, [2]Centre National de Recherches Météorologiques - UMR 3583 Météo France/CNRS, Toulouse, France

**Abstract** Several studies have pointed out the dependence of low-cloud feedbacks on the strength of the lower-tropospheric convective mixing. By analyzing a series of single-column model experiments run by a climate model using two different convective parametrizations, this study elucidates the physical mechanisms through which marine boundary-layer clouds depend on this mixing in the present-day climate and under surface warming. An increased lower-tropospheric convective mixing leads to a reduction of low-cloud fraction. However, the rate of decrease strongly depends on how the surface latent heat flux couples to the convective mixing and to boundary-layer cloud radiative effects: (i) on the one hand, the latent heat flux is enhanced by the lower-tropospheric drying induced by the convective mixing, which damps the reduction of the low-cloud fraction, (ii) on the other hand, the latent heat flux is reduced as the lower troposphere stabilizes under the effect of reduced low-cloud radiative cooling, which enhances the reduction of the low-cloud fraction. The relative importance of these two different processes depends on the closure of the convective parameterization. The convective scheme that favors the coupling between latent heat flux and low-cloud radiative cooling exhibits a stronger sensitivity of low-clouds to convective mixing in the present-day climate, and a stronger low-cloud feedback in response to surface warming. In this model, the low-cloud feedback is stronger when the present-day convective mixing is weaker and when present-day clouds are shallower and more radiatively active. The implications of these insights for constraining the strength of low-cloud feedbacks observationally is discussed.

## 1. Introduction

Since the pioneering climate change assessment of *Charney et al.* [1979], climate model estimates of the *Equilibrium Climate Sensitivity* (ECS) vary from roughly 1.5 K to 4.5 K of global surface warming per equivalent doubling of $CO_2$ concentration in the atmosphere [*Randall et al.*, 2007; *IPCC*, 2013]. This large inter-model spread is known to arise primarily from differences in tropical and subtropical marine boundary-layer cloud responses to a warming climate, which results in a wide range of simulated cloud radiative feedbacks [*Bony and Dufresne*, 2005; *Webb et al.*, 2006; *Vial et al.*, 2013; *Zelinka et al.*, 2013].

In recent years, progress has been made in identifying the physical mechanisms which underly the response of low-clouds to global warming. The analysis of low-cloud feedback processes through a hierarchy of numerical models [*Wyant et al.*, 2009; *Rieck et al.*, 2012; *Blossey et al.*, 2013; *Bretherton et al.*, 2013; *Brient and Bony*, 2013; *Webb and Lock*, 2013; *Zhang et al.*, 2013; *Bretherton*, 2015] showed that the sign and amplitude of the low-cloud feedback depend, at first order, on two competing mechanisms. On the one hand, enhanced moistening by surface turbulent fluxes and reduced subsidence tend to increase the low-cloud fraction and to produce a negative radiative cloud feedback [*Rieck et al.*, 2012; *Webb and Lock*, 2013; *Zhang et al.*, 2013]. On the other hand, enhanced drying of the boundary-layer by shallow convection tends to decrease the cloud fraction and leads to a positive radiative cloud feedback [*Rieck et al.*, 2012; *Bretherton et al.*, 2013; *Zhang et al.*, 2013; *Sherwood et al.*, 2014].

Potential constraints on low-level cloud feedbacks and ECS estimates have emerged from these process-oriented studies, and also from more statistical-oriented approaches. In particular, several studies support the idea that the representation of the present-day lower-tropospheric convective mixing in climate models could explain a large amount of the inter-model spread in ECS estimates by affecting the low-level cloud

feedback [*Gettelman et al*., 2012; *Sherwood et al*., 2014; *Tomassini et al*., 2014; *Brient et al*., 2016]. By mixing the air between a moist boundary-layer and a comparatively drier free troposphere, the lower-tropospheric mixing reduces the humidity gradient of the lower troposphere. In a warmer climate, and for a given convective mass flux, the mixing is expected to strengthen owing to the enhanced humidity gradient in the lower troposphere (a consequence of the nonlinear Clausius-Clapeyron relationship), and thus to dry the boundary-layer more efficiently, yielding a reduced low-cloud fraction and a positive low-cloud feedback. Since the rate of drying of the boundary-layer is assumed to be proportional to the strength of the present-day convective mixing (for a given convective mass flux), models with stronger mixing in the current climate would exhibit a stronger low-level cloud feedback [*Sherwood et al*., 2014]. *Brient et al*. [2016] further showed that the vertical structure of boundary-layer cloudiness, which seems to be intimately connected to the strength of the convective mixing, might also constitute a potential constraint on low-level cloud feedbacks and ECS estimates. However, more direct model experimentation (as in *Tomassini et al*. [2014] and *Kamae et al*. [2016]) does not always yield significant correlation between ECS and indicators of the lower-tropospheric mixing, such as tropospheric relative humidity (as in *Fasullo and Trenberth* [2012]) or vertical gradients in temperature, relative humidity and vertical velocity (as in *Sherwood et al*. [2014]). This inconsistency between multimodel ensemble studies [e.g., *Sherwood et al*., 2014; *Brient et al*., 2016] and single-model experimentation studies [e.g., *Tomassini et al*., 2014; *Kamae et al*., 2016] seems to depend on the ensemble of model simulations analyzed [*Kamae et al*., 2016]. Therefore, it suggests that our comprehension of the mechanisms that relate boundary-layer drying and low-level cloud reduction with climate warming to the strength of the present-day convective mixing is incomplete.

In this study, we step back to a more idealized framework to understand how parameterized shallow convective mixing controls the present-day representation of marine boundary-layer shallow cumulus clouds and the low-cloud feedback in a warmer climate. For this purpose, we use the IPSL-CM5A-LR climate model, and explore an ensemble of sensitivity experiments (in which convection scheme parameters are perturbed) using single-column configurations of this model under the CFMIP-GASS Intercomparison of large-eddy models and single-column models (CGILS) protocol [*Zhang et al*., 2012]. Using a Single-Column Model (SCM) allows us to decouple the model physics from the large-scale dynamics, and therefore to simplify the problem. The IPSL-CM5A-LR climate model is a useful tool in that respect, since it simulates similar low-cloud properties (i.e., vertical distribution, fraction and radiative forcing) in the SCM as in its parent GCM [*Brient and Bony*, 2012, 2013].

After a description of the model and of the experimental protocol (section 2), we show (i) that the relationship between the shallow convective mixing and low-level clouds in the present-day climate depends on two mechanisms (section 3), and (ii) how the understanding of these present-day relationships can help understand the low-cloud feedback predicted by the model (in section 4). A conclusion is presented in section 5.

## 2. Model and Experimental Design

### 2.1. Brief Model Description

The IPSL-CM5A-LR climate model [*Dufresne et al*., 2013], which has participated in the CMIP5 model intercomparison, is run with the LMDZ4 atmospheric model [*Hourdin et al*., 2006] at a $2.5^\circ \times 1.875^\circ$ longitude/latitude horizontal resolution and 39 vertical levels including 8 levels below 2 km. Turbulent transport in the planetary boundary layer is treated as a vertical diffusion with an eddy diffusion coefficient depending on the local stability (through the Richardson number) and on the mixing length [*Laval et al*., 1981]. The model is usually run with the Emanuel convection scheme (*Emanuel*, 1991, modified by *Emanuel* [1993] and *Grandpeix et al*. [2004]), but it can also be run with the Tiedtke scheme [*Tiedtke*, 1989], as for instance in *Bony et al*. [2004]; this study uses these two convective schemes, having very different closures: the former is based on a stability closure (the convective avalaible potential energy, CAPE) - this version of the model is referred to as LMDs, and the later on a subcloud moisture convergence closure (we refer to this version as LMDc).

While nonconvective clouds are predicted in the same way whatever the convective scheme used, the parametrization of clouds associated with cumulus convection depends on the convective scheme used in the model. The analysis presented here is done by activating only the nonconvective cloud scheme, although the results are qualitatively similar when activating both convective and nonconvective cloud

schemes. This implies that the dependence of the low-cloud amount on convection scheme is primarily related to the interaction between the convective scheme and large-scale variables of temperature and humidity, rather than to the formulation of the cloud schemes. An extended description of the physical parameterizations that are relevant for the representation of boundary-layer clouds in this model is given in Appendix A.

### 2.2. Idealized Single-Column Model Simulations

To investigate the link between the lower-tropospheric convective mixing and marine shallow cumulus clouds, we use single-column configurations of the IPSL-CM5A-LR model under the CGILS protocol [*Zhang et al*., 2012, 2013]. The CGILS project has been initiated and thereafter widely used to understand the physical mechanisms of marine-boundary layer cloud feedbacks through single-column, cloud-resolving and large-eddy models under idealized large-scale forcing conditions that are representative of subsident regimes [*Zhang et al*., 2012, 2013; *Bretherton et al*., 2013; *Brient and Bony*, 2013]. In this study we focus on the trade-wind shallow cumulus regime (so-called "S6 regime" of CGILS, located at 17°N and 149°W). The forcing data include the large-scale horizontal advective tendencies of temperature and water vapor, vertical velocity and surface boundary conditions. In subsiding regions, the vertical pressure velocity is derived based on the clear-sky thermodynamic equation in the free-troposphere, in which subsidence warming and horizontal advection are balanced by radiative cooling. More specifically, the vertical velocity is derived by specifying its shape (using the function given in *Zhang et al*. [2012]) and constraining its amplitude as budget residual using the vertically integrated (from 900 hPa to 300 hPa) horizontal temperature tendency from ERA-Interim data [*Dee et al*., 2011] and net clear-sky radiative cooling (calculated using the RRTM radiation code [*Mlawer et al*., 1997]). Moreover, a stochastic variability is applied on the vertical profile, in order to better reproduce the vertical cloud distribution simulated by the parent GCM [*Brient and Bony*, 2013]. In the free troposphere (above 800 hPa), horizontal advective tendencies of temperature and water vapor are obtained as residuals from the clear-sky thermodynamic and humidity equations. Below 900 hPa, they are calculated using the SST spatial gradient, surface relative humidity and surface winds from ERA-Interim, and between 800 and 900 hPa, they are linearly interpolated (as explained in *Zhang et al*. [2012]). In the present-day climate, the SCM is run with a SST of 298.8 K, a surface pressure of 1014.1 mbar, zonal and meridional surface winds of $-7.4\,\mathrm{m\,s^{-1}}$ and $-2.7\,\mathrm{m\,s^{-1}}$, respectively, a mean solar downward radiation at the top of the atmosphere (TOA) of $448.1\,\mathrm{W\,m^{-2}}$ and no diurnal cycle. For the perturbed simulation, the SST is raised by 2 K and the large-scale forcing (horizontal advective tendencies and vertical velocity) remain unchanged, which allows us to isolate the response of low-clouds to the increased convective mixing that results from thermodynamics rather than from a change in dynamics [see also *Bretherton et al*., 2013]. A comprehensive description of the CGILS project is given in *Zhang et al*. [2012].

### 2.3. Perturbing the Convective Mixing

To assess the sensitivity of cloud properties (i.e., fraction, water content and radiative forcing) to variations of the lower-tropospheric convective mixing, we perform a series of sensitivity experiments in which we perturb the parameters of the convection schemes that control the intensity of the convection for a given large-scale forcing (i.e., horizontal advective tendencies and vertical velocity remain unchanged across the experiments).

A first set of experiments consists of multiplying the convective mass flux at cloud base by an artificial coefficient (referred to as $k$; the control experiment corresponds to $k = 1$). In practice, the cloud-base mass flux is parametrized through a closure assumption that determines the intensity of the convection. When the coefficient is increased, the overall amplitude of the convection is enhanced. The range of variation of $k$ depends on the convection scheme: $k = [0.6, 2]$ when using $LMD_s$ and $k = [0.6, 1]$ with $LMD_c$. When using $LMD_c$, we do not consider coefficients greater than 1, because for larger values, the convection becomes strong enough to produce large amount of rainfall. Clouds are deeper and their cloud-base is higher so that the CGILS S6 setup is likely not the most appropriate for this kind of regime. Besides, *Bretherton et al*. [2013] have shown in large-eddy simulations that precipitation could promote other feedback processes that affect the vertical structure of boundary-layer shallow cumulus clouds. Although precipitation might be an important aspect of the relationship between convective mixing and shallow cumulus clouds, we do not address it in the present study as it would require a more complex framework. We leave this point for future studies. The lower bound is fixed at 0.6 for ease of readability on the graphical outputs.

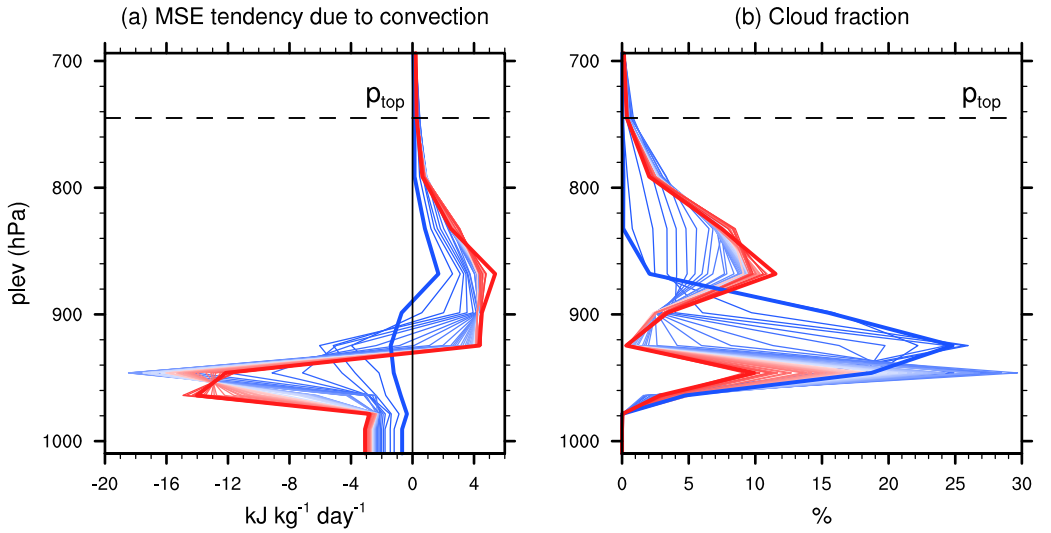


**Figure 1.** (a) Vertical distribution of moist static energy flux convergence due to convection ($-\partial_p\overline{\omega' h'}$, in kJ kg$^{-1}$ d$^{-1}$), computed from model tendencies and (b) cloud fraction (in %) for all range of parameters $k$ (i.e., $0.05 < k < 2$) using $LMD_s$. Profiles corresponding to the minimum value of $k$ are shown in thick blue, and to the maximum value in thick red; intermediate values of $k$ are represented by the blue-to-red curves. The dashed line represents the top of the boundary-layer at $p_{top} \simeq 750$ hPa.

A second set of experiments is run, which consists in modulating a tunable parameter of the model that controls (i) the efficiency of convective precipitation when using $LMD_s$ (details in Appendix B) and (ii) the rate of lateral entrainment/detrainment for the shallow convection when using $LMD_c$ (as in *Tomassini et al.* [2014]). The results are qualitatively similar to the $k$-experiments, and are not shown.

Convective mixing is analyzed through the vertical transport of moist static energy (MSE, in *J/kg*). MSE, defined as $h = c_p T + gz + L_v q$, characterizes the energy of an air parcel associated with enthalpy at temperature T (in K) and heat capacity at constant pressure ($c_p = 1004\,\mathrm{J/(K\,kg)}$), gravitational potential energy at height z (in m) and standard acceleration due to gravity ($g = 9.81\,\mathrm{m\,s^{-2}}$) and latent energy at specific humidity q (in kg/kg) and latent heat of vaporization ($L_v = 2.5\times10^6\,\mathrm{J/kg}$). The MSE input in the atmosphere by surface turbulent fluxes is balanced by all the other processes. In trade-wind cumulus regime, as considered here, the dominant processes are: clear-sky and cloudy radiative cooling, vertical mixing by convective fluxes, advection of low-MSE air from the free troposphere by large-scale subsidence, and MSE export toward more active convective regions by the large-scale horizontal winds. Note that conservation of MSE during phase changes (including condensation and evaporation), makes it a useful indicator to study processes such as the lower-tropospheric mixing in the presence of clouds and precipitation.

An illustration of the MSE mixing by convection and its impact on the vertical distribution of clouds is shown for $LMD_s$ in Figure 1 (analyzed in detail in section 3). Convective mixing decreases MSE at low atmospheric levels (up to $\sim$ 900 hPa) and increases MSE higher up (up to $\sim$ 750 hPa). As $k$ is increased, this convective tendency is amplified (Figure 1a), and is associated with deeper clouds and a reduced cloud fraction at low levels (Figure 1b).

To measure the strength of the convective mixing, we introduce a *Convective Mixing Index* ($\mu$), which characterizes the strength of the convective transport of MSE within the lower troposphere (Figure 1a) as:

$$\begin{aligned}\mu &= \int_{p_1}^{p_{top}} \left(-\partial_p \overline{\omega' h'}|_{con}\right)\frac{dp}{g} - \int_{p_0}^{p_1}\left(-\partial_p \overline{\omega' h'}|_{con}\right)\frac{dp}{g} \\ &= 2\overline{\omega' h'}|_{con}(p_1)\end{aligned} \tag{1}$$

where $-\partial_p\overline{\omega' h'}|_{con}$ denotes the vertical convergence of the MSE flux associated with cumulus convection (computed from model tendencies–Figure 1a). $p_0$ is the pressure of the first model level and $p_{top}$ is the pressure level at the top of the boundary-layer, near 750 hPa–the top of the simulated boundary-layer clouds (Figure 1b) and of the convective activity (Figure 1a). $p_1$ is defined as the model level where the convective tendency vanishes (or where the upward convective flux of MSE is maximum). Note that

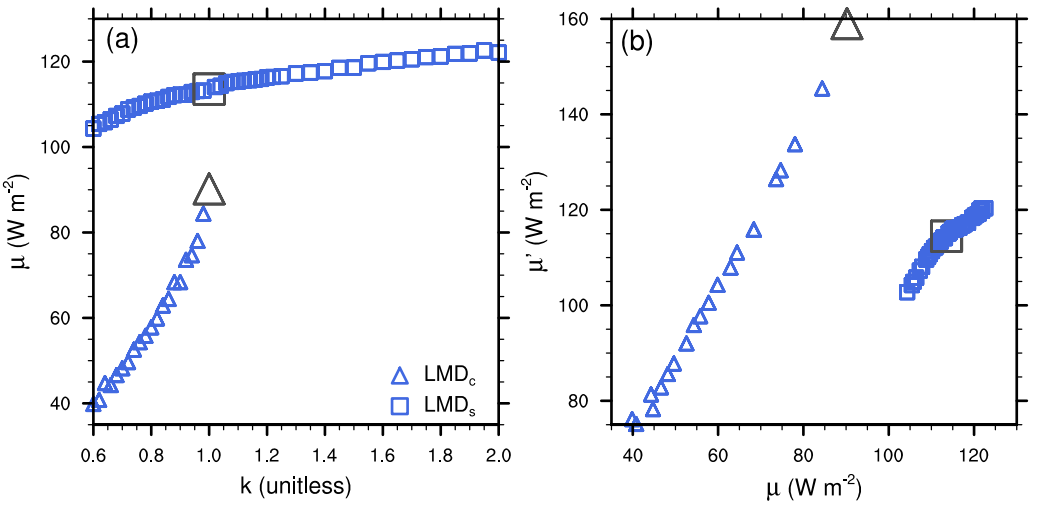


**Figure 2.** (a) Convective mixing index computed from model tendency ($\mu$, in W/m$^{-2}$) as a function of the parameter k. (b) Relationship between $\mu$ and $\mu'$ (approximation of $\mu$ using the convective mass flux and deficit of MSE-see section 2.3). Results are shown for $LMD_s$ (open squares) and $LMD_c$ (open triangle). Here and in subsequent figures, the control experiment (when k = 1) is shown by the larger dark marker.

because the total integral of the convective MSE tendency is zero, the first and second term in equation (1) equal each other, and each equals the peak upward flux of MSE at $p_1$ (i.e., $\overline{\omega' h'}|_{con}(p_1)$). Units of $\mu$ are in W/m$^{-2}$.

Although the convective mixing generally increases as $k$ is increased, its sensitivity to the parameter $k$ depends on the convective scheme (Figure 2a): there is a more rapid increase in $\mu$ when using $LMD_c$ than $LMD_s$, and on average $LMD_s$ produces stronger convective mixings ($\mu \sim 108$ W/m$^{-2}$ for the control experiment - when k = 1) than $LMD_c$ ($\mu \sim 88$ W/m$^{-2}$ for k = 1). The reason explaining these different sensitivities in convective mixing is presumably related to different feedback processes acting on $\mu$, either through the diagnosed mass flux or the MSE contrast. In this study, the variations in $\mu$ with $k$ are explained to a large extent by changes in the mass flux (not shown). One of these feedbacks could operate through the closure assumption for convective parametrizations, which determines (among other things) the rate of increase in the mass flux as a function of convective instability. When using $LMD_s$, the convective mass flux at cloud-base ($M_b$) is roughly parametrized as $M_b \propto \sqrt{CAPE}$ [see in *Emanuel*, 1991, equation (17a)], so that the rate of increase in $M_b$ as a function of $CAPE$ is inversely proportional to convective intensity (i.e., $dM_b \propto \frac{1}{2M_b} dCAPE$). In $LMD_c$, the closure in moisture convergence relies on a more linear relationship between $M_b$ and latent heat flux ($E$): $M_b \propto E$ [see *Tiedtke*, 1989, equation (19)], so that $dM_b \propto dE$. Both CAPE (in $LMD_s$) and E (in $LMD_c$) are roughly linearly related to the parameter $k$, with a similar rate of increase (i.e., $dE \sim dCAPE \propto dk$ - not shown). This thus suggests that the different sensitivities in $\mu$ to the parameter $k$ can be explained, to some extent, by the functional form of how $M_b$ depends on convective instability: at first order, the first type of closure favors a slower rate of increase in $\mu$ with $k$ than the second type of closure.

Although $\mu$ characterizes the *true* value of the convective mixing of the model (as it is based on model tendencies), it is also desirable to have a measure that can be applied to other climate models (i.e., model tendencies are not included in the standard output of CMIP5 models) and observations (see discussion in section 5). Such a measure could be obtained from the mass-flux approximation [*Yanai et al.*, 1973], which defines the vertical profile of the convective eddy flux as $F = gM(h_0 - h)$, where $M$ is the net convective mass flux, $h$ the vertical profile of MSE and $h_0$ the MSE at the first vertical level (an approximation of the MSE within the updraft). Estimates of convective mass flux have recently been obtained in observations using subcloud layer budget analyses [e.g., *Masunaga and Luo*, 2016] or by estimating convective drafts from Doppler velocity measurements in nonprecipitating cumuli [e.g., *Lamer et al.*, 2015]. Taking the vertical divergence of $F$ and applying equation (1) yields an approximation of $\mu$ (referred to as $\mu'$ in equation (2)) that is linearly related to $\mu$: $\mu' \simeq \mu$ for $LMD_s$ and $\mu' \simeq 2\mu$ for $LMD_c$ (Figure 2b).

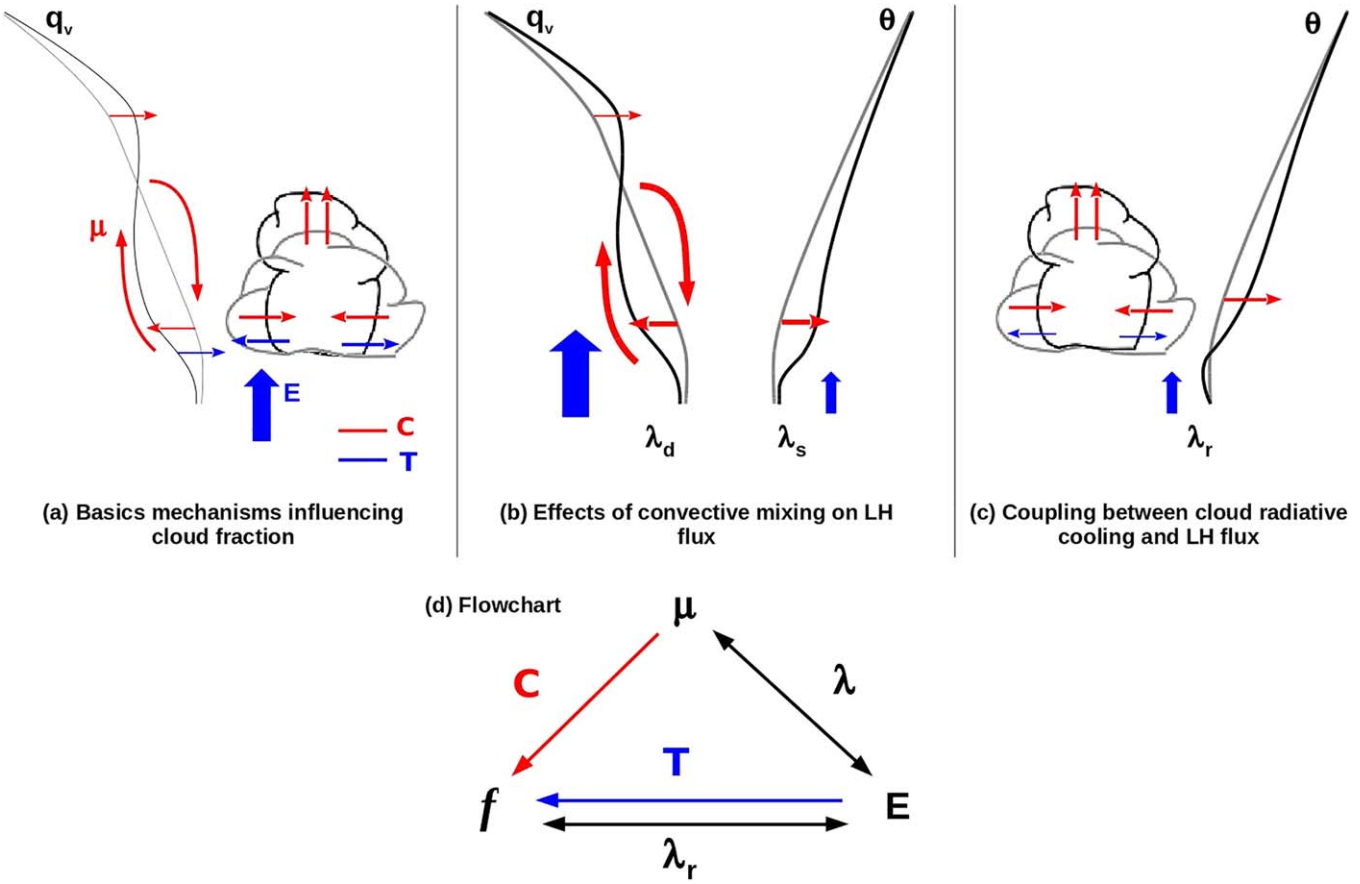


**Figure 3.** Illustration of the five mechanisms underlying the sensitivity in cloud amount to convective mixing. $\mathcal{C}$ (in red) and $\mathcal{T}$ (in blue) are two basic processes affecting boundary-layer cloud fraction (*f*: CF averaged through the depth of the boundary-layer in Figure 1b) in opposite directions: $\mathcal{C}$ represents the reduced cloud amount as convective mixing increases, while $\mathcal{T}$ is the increase in cloud amount associated with enhanced turbulent surface flux of moisture. Latent heat flux can then be damped or strengthened through $\mathcal{T}$ by three feedback loops, namely $\lambda_d$, $\lambda_s$ and $\lambda_r$. $\lambda_d$ represents the coupling between $\mu$ and latent heat flux, which strengthens latent heat flux (larger blue arrow) through $\mathcal{T}$, thus damping the reduction of *f* initially induced by convective mixing ($\mathcal{C}$). $\lambda_s$ is also part of the coupling between $\mu$ and latent heat flux, which damps latent heat flux (smaller blue arrow) through $\mathcal{T}$ and thus enhances the reduction of *f* induced by $\mathcal{C}$. $\lambda_r$ represents the coupling between boundary-layer clouds (through their radiative cooling) and latent heat flux, which damps latent heat flux (smaller blue arrow) through $\mathcal{T}$ and enhances the reduction of *f* induced by $\mathcal{C}$. In Figure 3b, $\lambda = \lambda_d + \lambda_s$.

$$\mu' = \int_{p_1}^{p_{top}} \partial_p[M(h-h_0)]dp - \int_{p_0}^{p_1} \partial_p[M(h-h_0)]dp \quad (2)$$

The analysis presented here is done by using $\mu$, although the results are qualitatively similar using both measures of the convective mixing. Note also that only the amplitude of the mass flux varies across the experiments, while its vertical structure remains roughly constant with *k*. As a result, *M* can be approximated as $M(k,p) = M_b(k)\Phi(p)$, where $M_b(k)$ is the net mass flux at cloud base that depends on *k* and $\Phi(p)$ contains all information about the vertical structure of the mass flux for $k = 1$.

In section 3, we investigate the physical mechanisms that control the sensitivity of low-clouds to convective mixing, and its dependence on the convection scheme. The implications of these relationships for understanding low-cloud feedback uncertainties in a warmer climate are addressed in section 4.

## 3. Interplay Between Convective Mixing, Low-Level Clouds and Surface Fluxes

### 3.1. Framework

Recent studies suggest that boundary-layer clouds are influenced by two main competing mechanisms (illustrated in Figure 3a). First, by exporting moisture from the lower troposphere to the free troposphere, shallow convective mixing tends to deepen boundary-layer clouds and to dry the low troposphere, which reduces the cloud fraction at lowest levels [*Stevens*, 2007; *Rieck et al.*, 2012; *Zhang et al.*, 2013; *Sherwood*

**Table 1.** List of Coefficients With Their Physical Description and Value Estimated From Multiple Least-Squares Regression (See Appendix C) for CRE ON and CRE OFF (into Parentheses) Experiments[a]

| Coefficients | Physical Description | $LMD_s$ | $LMD_c$ |
|---|---|---|---|
| $\mathcal{C} \equiv \frac{\partial f}{\partial \mu}\Big\vert_E$ | Rate of decrease in boundary-layer cloud fraction for a unit increase in convective mixing (at constant latent heat flux) | −0.074 (−0.046) | −0.010 (−0.025) |
| | *Standardized coefficient* | *−0.823 (−1.017)* | *−1.094 (−1.187)* |
| $\mathcal{T} \equiv \frac{\partial f}{\partial E}\Big\vert_\mu$ | Rate of increase in boundary-layer cloud fraction for a unit increase in latent heat flux (at constant mixing) | 0.133 (0.012) | 0.018 (0.057) |
| | *Standardized coefficient* | *0.179 (0.020)* | *0.113 (0.198)* |
| $\lambda = \lambda_d + \lambda_s$ | Rate of change in latent heat flux for a unit increase in convective mixing (at constant cloud radiative forcing): latent heat flux is enhanced through convective drying $\left(\lambda_d \equiv \frac{\partial E}{\partial q_0}\Big\vert_{k_0} \frac{dq_0}{d\mu}\Big\vert_R\right)$ and reduced through increased stability induced by convective warming $\left(\lambda_s \equiv \frac{\partial E}{\partial k_0}\Big\vert_{q_0} \frac{dk_0}{d\mu}\Big\vert_R\right)$ | 0.014 (0.071) | 0.058 (0.073) |
| | *Standardized coefficient* | *0.117 (0.987)* | *1.018 (0.975)* |
| $\lambda_r \equiv \frac{\partial E}{\partial k_0}\Big\vert_{q_0} \frac{dk_0}{dR}\Big\vert_\mu$ | Rate of change in latent heat flux for a unit change in cloud radiative forcing (at constant mixing) | 0.364 | 0.423 |
| | *Standardized coefficient* | *1.102* | *0.093* |
| $\alpha = \frac{dR}{df}$ | Sensitivity of cloud radiative forcing to boundary-layer cloud fraction | 4.051 | 0.488 |
| $\alpha\mathcal{C}\lambda_r$ | | −0.109 | −0.002 |
| $R^2$ for *df* in equation (3) | | 0.993 (0.994) | 0.964 (0.990) |
| $R^2$ for *dE* in equation (4) | | 0.973 (0.974) | 0.995 (0.950) |

[a]Values in italics are the standardized coefficients (definition given in Appendix C); they provide the relative weight of the coefficients in their respective equations. The last two lines show the total fraction of variance in *df* and *dE* explained using the parameters $\mathcal{C}$ and $\mathcal{T}$ in equation (3) and $\lambda$ and $\lambda_r$ in equation (4), respectively.

*et al*., 2014; *Brient et al*., 2016]. The second mechanism is the turbulent moistening through evaporation from the ocean, which moistens the lower troposphere and enhances the low-level cloud amount [*Rieck et al*., 2012; *Webb and Lock*, 2013; *Zhang et al*., 2013; *Brient et al*., 2016].

Therefore, as a first-order approximation, we assume that the variation in boundary-layer cloud fraction ($f$) is only a function of the convective mixing ($\mu$) and latent heat flux ($E$). Here, we quantify this relationship through a multiple regression framework (equation (3)) as:

$$df = \mathcal{C}d\mu + \mathcal{T}dE \tag{3}$$

where $f$ is the averaged cloud fraction through the depth of the boundary-layer (up to $p_{top}$), and $\mathcal{C} \equiv \frac{\partial f}{\partial \mu}\Big\vert_E < 0$ and $\mathcal{T} \equiv \frac{\partial f}{\partial E}\Big\vert_\mu > 0$ are the partial regression coefficients (cf. Table 1) based on multiple least-squares regression of $df$ against $d\mu$ and $dE$ (details in Appendix C).

However, many studies have shown that convective and latent heat fluxes are coupled to each other [e.g., *Tiedtke*, 1989]. Therefore, the impact of convective mixing on low-level cloud fraction is partly related to its impact on latent heat flux. The experimental protocol presented in this study allows us to identify two feedback mechanisms that can enhance or reduce the latent heat flux, and explain why the sensitivity of the low-cloud amount to convective mixing can depend on convective parameterization.

The latent heat flux is commonly expressed as $E(k_0,q_0) = \rho L_v U k_0(q_s - q_0)$, where the density of air ($\rho$), near-surface wind ($U$) and saturated specific humidity at sea surface temperature ($q_s$) are kept constant in the CGILS experimental framework. The first mechanism (left side of Figure 3b) involves the near-surface specific humidity ($q_0$) that depends on convective mixing through the lower-tropospheric convective drying: as $\mu$ increases, low-level convective drying enhances the latent heat flux (through a decrease in $q_0$), which in turn damps the reduction of the low-cloud amount initially induced by convective mixing (equation (3)). The second mechanism (right side of Figure 3b) involves the turbulent exchange coefficient for moisture ($k_0$) that depends inversely on stability (through the Richardson number in the IPSL model). More intense convective warming as $\mu$ increases, stabilizes the lower troposphere, thus yielding a reduced latent heat flux (through a decrease in $k_0$). In addition, low-cloud radiative cooling was shown to interact strongly with surface fluxes [*Fermepin and Bony*, 2014]. Here, we show that this interaction operates through $k_0$. At low atmospheric levels, the weakened cloud radiative cooling (initially induced by convective mixing) also

stabilizes the lower troposphere, yielding a weaker latent heat flux. By reducing the moisture input, the decreased latent heat flux strengthens the decrease in low-cloud fraction and cloud radiative cooling (through $\mathcal{T}$ in equation (3)). This last mechanism is illustrated in Figure 3c.

Now, we assume that $q_0$ and $k_0$ are functions of the convective mixing and the net boundary-layer cloud radiative effect (R), which is essentially driven by the longwave cloud radiative cooling (R > 0 by convention): $q_0 = q_0(\mu)$ and $k_0 = k_0(\mu, R)$. We also assume that $dR$ is linearly related to $df$ (which is a good approximation for the IPSL model), so that $dR = \alpha df = \alpha\ \mathcal{C} d\mu + \alpha\ \mathcal{T} dE$. Thus, we can express the change in latent heat flux as:

$$\begin{aligned} dE &= \left.\frac{\partial E}{\partial q_0}\right|_{k_0} dq_0 + \left.\frac{\partial E}{\partial k_0}\right|_{q_0} dk_0 \\ &= \left.\frac{\partial E}{\partial q_0}\right|_{k_0} \left.\frac{\partial q_0}{\partial \mu}\right|_R d\mu + \left.\frac{\partial E}{\partial k_0}\right|_{q_0} \left.\frac{\partial k_0}{\partial \mu}\right|_R d\mu + \left.\frac{\partial E}{\partial k_0}\right|_{q_0} \left.\frac{\partial k_0}{\partial R}\right|_\mu dR \\ &= \frac{1}{1-\alpha\mathcal{T}\lambda_r}(\lambda_d + \lambda_s + \alpha\mathcal{C}\lambda_r) d\mu \end{aligned} \tag{4}$$

where $\lambda_d \equiv \left.\frac{\partial E}{\partial q_0}\right|_{k_0} \left.\frac{dq_0}{d\mu}\right|_R > 0$, $\lambda_s \equiv \left.\frac{\partial E}{\partial k_0}\right|_{q_0} \left.\frac{dk_0}{d\mu}\right|_R < 0$ and $\lambda_r \equiv \left.\frac{\partial E}{\partial k_0}\right|_{q_0} \left.\frac{dk_0}{dR}\right|_\mu > 0$, and with $\left.\frac{\partial E}{\partial q_0}\right|_{k_0} > 0$, $\left.\frac{dq_0}{d\mu}\right|_R < 0$, $\left.\frac{\partial E}{\partial k_0}\right|_{q_0} > 0$, $\left.\frac{dk_0}{d\mu}\right|_R < 0$ and $\left.\frac{dk_0}{dR}\right|_\mu > 0$.

For simplicity, in the rest of the paper, we will often refer to the total effect of convective mixing on latent heat flux ($\lambda$) as $\lambda = \lambda_d + \lambda_s$. Note that the sign of these coefficients, expected from the physical arguments discussed previously, are consistent with estimates of $\lambda$ and $\lambda_r$ (cf. Table 1) inferred from the multiple least-squares regression of $dE$ against $d\mu$ and $dR$ (details in Appendix C).

Equation (4) describes how the latent heat flux depends on convective mixing: directly through the convective fluxes of temperature and water vapor ($\lambda$) and indirectly, through the radiative cooling of low-level clouds ($\alpha\mathcal{C}\lambda_r$).

By replacing $dE$ into equation (3), the sensitivity of the boundary-layer cloud fraction ($f$) to a change in convective mixing can be expressed as:

$$\begin{aligned} df &= \left[\mathcal{C} + \frac{1}{1-\alpha\mathcal{T}\lambda_r}\mathcal{T}(\lambda_d + \lambda_s + \alpha\mathcal{C}\lambda_r)\right] d\mu \\ &\simeq [\mathcal{C} + \mathcal{T}(\lambda_d + \lambda_s + \alpha\mathcal{C}\lambda_r)] d\mu \\ &\simeq [\mathcal{C} + \mathcal{T}(\lambda + \alpha\mathcal{C}\lambda_r)] d\mu \end{aligned} \tag{5}$$

Note that we have omitted the term $\frac{1}{1-\alpha\mathcal{T}\lambda_r}$ in equation (5), as $\alpha\mathcal{T}\lambda_r \ll 1$ (Table 1) and therefore it does not significantly affect the results (see Appendix C).

These two terms ($\lambda$ and $\alpha\mathcal{C}\lambda_r$) will now be investigated in more detail. In particular, we will show that their relative importance in equation (5) partly explains the differences in the sensitivity of boundary-layer clouds to convective mixing among the convective schemes.

### 3.2. Coupling Between Convective Mixing and Latent Heat Flux ($\lambda$)

To investigate the direct coupling between convective mixing and latent heat flux (i.e., $\lambda_d$ and $\lambda_s$ in equation (4)), we ran the same simulations as described in section 2.3, but with the radiative effects of clouds switched off (referred to as CRE OFF), as done in the COOKIE project (Clouds On/Off Klimate Intercomparison Experiment [*Stevens et al.*, 2012]). In doing so, the feedback between cloud radiative cooling and latent heat flux is switched off ($\lambda_r = 0$ in equations (4) and (5)), thus allowing us to analyze how $\lambda$ alone couples the convective mixing to the latent heat flux and the boundary-layer cloud fraction.

As $\mu$ increases, convection exports moisture from lower atmospheric levels to the upper part of the boundary-layer (Figures 4a and 4f), yielding deeper clouds and a reduced cloud fraction at lowest levels (Figures 4c and 4h) through $\mathcal{C}$ (equation (5)). Moreover, the sign of $\lambda$ depends on how strongly the convection scheme stabilizes the lower troposphere ($\lambda_s$) with respect to convective drying ($\lambda_d$): it is positive if $|\lambda_d| > |\lambda_s|$, and negative otherwise. Therefore, an increase of the mixing enhances E and weakens the

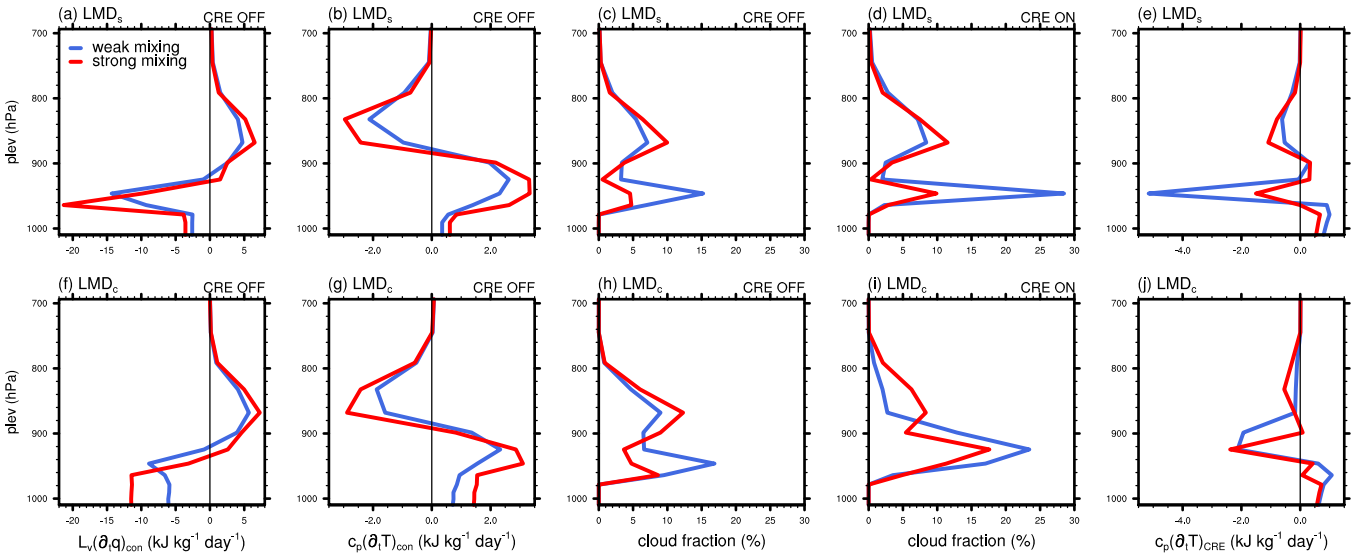


**Figure 4.** Vertical profiles for $LMD_s$ (top row) and $LMD_c$ (bottom row) of: (from left to right) (a, f) humidity and (b, g) temperature tendencies due to convection (in kJ kg$^{-1}$ d$^{-1}$) when the cloud radiative forcing is turned off (CRE OFF experiments), cloud fraction (in %) for (c, h) CRE OFF and (d, i) CRE ON experiments and (e, j) temperature tendency due to cloud radiative effects (CRE ON - CRE OFF, in kJ kg$^{-1}$ d$^{-1}$). The blue line corresponds to weak mixing (when k = 0.6), and the red line to strong mixing (k = 2 for $LMD_s$ and k = 1 for $LMD_c$).

reduction of $f$ in the former case, while it weakens E and strengthens $df$ (i.e., the reduction of $f$) in the latter case (through $\mathcal{T}$ in equation (5)).

In the IPSL model, both processes are at play. As convection dries the lower troposphere (Figures 4a and 4f), the humidity gradient between the surface (which is constrained by the fixed SST) and the first layer increases, yielding a decreased $q_0$, and thus an increased turbulent transport of moisture (Figures 5a and 5f–green markers). At the same time, $k_0$ is reduced as the lower troposphere stabilizes under the effect of convective mixing (Figures 5b and 5g–green markers). However, the variation of convective drying at low levels is more important than that of convective warming (compare temperature and humidity tendency profiles in Figure 4; see also Figure 3b), so more weight is given to $\lambda_d$ than to $\lambda_s$ (i.e., $\lambda \simeq \lambda_d$ is positive in Table 1). This yields an

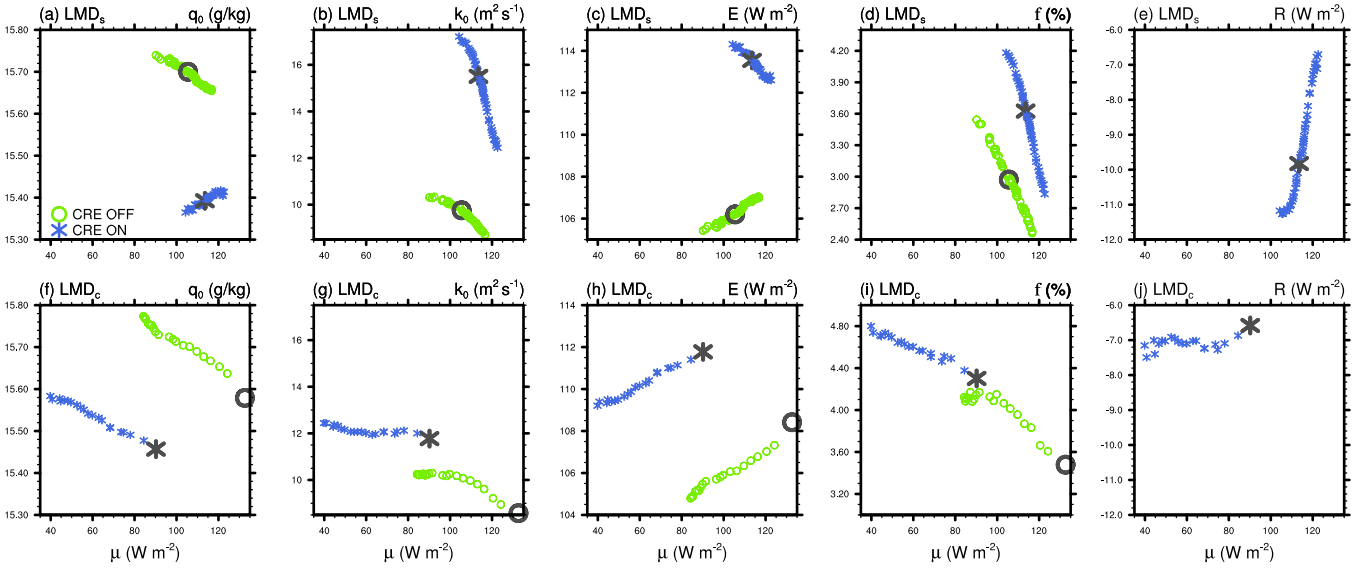


**Figure 5.** Dependence of different variables on $\mu$ for $LMD_s$ (top row) and $LMD_c$ (bottom row). From left to right: (a, f) specific humidity at the first vertical level ($q_0$, in g/kg), (b, g) turbulent exchange coefficient at low atmospheric levels ($k_0$, in m$^2$s$^{-1}$), vertical mass integral through the depth of the boundary-layer of (c, h) the turbulent diffusion flux for humidity ($E$, in W m$^{-2}$) and (e, j) the cloud radiative forcing ($R$, in W m$^{-2}$) and (d, i) boundary-layer cloud fraction ($f$, in %). Here and in subsequent figures, green markers correspond to CRE OFF experiments and blue markers to CRE ON experiments, and the large dark markers correspond to the control simulation (when k = 1). Note that the ranges of $y$ axes may not the same from one convective scheme to another, but the scales are the same.

enhanced latent heat flux as convective mixing is increased (Figures 5c and 5h–green markers), thus damping the decrease of low-cloud fraction initially induced by $\mathcal{C}$ (through $\mathcal{T}$ in equation (5)).

Note that although the two model versions predict similar $\lambda$ in the absence of cloud-radiative effects (Table 1 and slopes of the green curves in Figures 5c and 5h), the sensitivity of the cloud fraction to convective mixing is stronger in $LMD_s$ than in $LMD_c$ (compare the slopes of the green curves in Figures 5d and 5i). This is presumably explained by the fact that in $LMD_s$, the convective drying is maximum at the altitude of the low-cloud layer ($\sim$ 950 hPa), while in $LMD_c$ it is confined to altitudes that do not have any cloud to dessicate (Figures 4a and 4f). The amplitude of $\mathcal{C}$ is thus sensitive to the shape of the vertical profile of convective drying ($\mathcal{C}$ is stronger in $LMD_s$ than in $LMD_c$–Table 1). Note that although both convective drying and warming affect relative humidity and cloud fraction at low levels, the difference in $\mathcal{C}$ between the two convective schemes seems to be explained to a large extent by different convective drying (i.e., the two convective schemes differ primarily by their drying effect (Figures 4a and 4f) than their warming counterpart (Figures 4b and 4g)).

Therefore, in the absence of cloud radiative effects, the sensitivity of boundary-layer cloud fraction to convective mixing depends (i) on how strongly the convection scheme stabilizes the lower troposphere with respect to convective drying (which determines the sign of the coefficient $\lambda$), and (ii) on how efficient the lower-tropospheric convective mixing is at drying at levels of low-level clouds (which affects $\mathcal{C}$). The latter point explains the different sensitivities in low-level cloud fraction to convective mixing between the two convective schemes.

### 3.3. Coupling Between Low-Cloud Radiative Cooling and Latent Heat Flux ($\lambda_r$)

To demonstrate how $\lambda_r$ affects the relationship between convective mixing and low-clouds, we compare the CRE OFF experiments with the control experiments, in which clouds are radiatively active.

By cooling the cloud layer and warming the subcloud layer (Figure 4e and 4j), the low-cloud radiative cooling destabilizes the lower troposphere, yielding an increase in surface fluxes (see the jump in $k_0$ and latent heat flux between CRE OFF and CRE ON experiments in Figures 5b and 5g and Figures 5c and 5h, respectively).

In $LMD_s$, as the lower-tropospheric convective drying increases, the cloud fraction at lowest levels decreases (Figure 4d) and the associated radiative cooling weakens (Figure 4e), yielding decreased instability at low levels (compare green and blue markers in Figure 5b). This effect tends to reduce latent heat flux (i.e., $\lambda_r > 0$ in equation (4) and Table 1) and thus to oppose the effect of convective drying itself ($\lambda_d > 0$), and in this case even to reverse the sensitivity of latent heat flux to $\mu$ as illustrated in Figure 5c. We note also the slight increase in near-surface humidity in CRE ON experiments (Figure 5a, blue markers), which is an indication of the weaker upward turbulent transport of moisture within the lower troposphere. By reducing moisture input, the decreased latent heat flux enhances the decrease of low-level cloud fraction (blue slope steeper than green slope in Figure 5d). Moreover, the fact that E decreases with $\mu$ in CRE ON experiments suggests that E is more strongly related to low-level cloud radiative cooling than to the convective mixing (i.e., $|\alpha\mathcal{C}\lambda_r| > |\lambda|$), thus enhancing the decrease of low-level cloud fraction and cloud radiative cooling initially induced by the enhanced mixing ($\mathcal{C}$ in equation (5)).

However, in $LMD_c$, latent heat flux increases with $\mu$ in both CRE OFF and CRE ON experiments, which implies that E is more strongly related to the convective mixing than to low-level cloud radiative cooling (i.e., $|\lambda| > |\alpha\mathcal{C}\lambda_r|$ for this model). Indeed, the weak decrease in cloud radiative cooling with $\mu$ (Figure 5j) suggests a weak $\alpha\mathcal{C}\lambda_r$ in equation (4) (see also Figure 5g and Table 1). As a result, $f$ decreases less strongly as $\mu$ increases compared to $LMD_s$ (also because $\mathcal{C}$ is weaker in $LMD_c$–section 3.2 and Table 1).

Therefore, the relative importance of $\alpha\mathcal{C}\lambda_r$ and $\lambda$ explains to a large extent the different sensitivities in low-level cloud fraction to convective mixing between the two convective schemes. The more weight given to $\alpha\mathcal{C}\lambda_r$ with respect to $\lambda$, the stronger the reduction in $E$, and thus the stronger the weakening of low-level cloud fraction initially induced by the increased mixing (equation (5)).

### 3.4. Relative Contribution of $\lambda_r$ and $\lambda$

So far we have shown that both $\lambda_r$ and $\lambda$ are at play in the model, irrespective of the convective scheme. However, the importance of one mechanism relative to the other does depend on the convection scheme,

and partly explains the different sensitivities in boundary-layer clouds to convective mixing between both schemes (Figures 5d and 5i).

One reason that could explain a stronger contribution of $\alpha\mathcal{C}\lambda_r$ relative to that of $\lambda$ is related to the closure assumption used to determine the cloud base mass flux and the intensity of convection. In subsident regime, when using a closure in moisture convergence (e.g., $LMD_c$), the intensity of the convection is essentially dependent on surface turbulent fluxes. Therefore, we expect for this model the strength of the convective mixing to be primarily driven by surface latent heat flux. However, with a closure in CAPE (as for $LMD_s$), the intensity of the convection depends on the stratification of the atmosphere, and thus on differences between the actual profiles of temperature and moisture and the moist adiabatic profiles. In that case, both the surface and tropospheric fluxes of heat and moisture contribute to modulate the strength of the convection, including the vertical distribution of cloud radiative forcing. In particular, the radiative forcing associated with boundary-layer clouds, tends to enhance the CAPE by increasing the buoyancy of a rising cloud parcel. Therefore, when using $LMD_s$, we expect the convective mixing to be sensitive to variations in boundary-layer cloud forcing.

Following this line of reasoning, the sensitivity of the convective mixing to the cloud radiative forcing, which can be expressed as $\partial\mu/\partial R$, would to be stronger (at first order) for a closure in CAPE than a closure in moisture convergence. Therefore, by construction (i.e., $\frac{\partial\mu}{\partial R}=\frac{\partial\mu}{\partial E}\frac{\partial E}{\partial R}=\frac{\lambda_r}{\lambda}$), a convective scheme that uses a closure in CAPE gives more weight to $\lambda_r$ relative to that of $\lambda$ than a convective scheme that uses a closure in moisture convergence, and thus promotes a stronger sensitivity of low-level clouds to convective mixing. This is supported by values of $\lambda_r$ and $\lambda$ in Table 1: $\frac{\lambda_r}{\lambda}\simeq 26$ in $LMD_s$ and $\frac{\lambda_r}{\lambda}\simeq 7$ in $LMD_c$ (see also standardized coefficients in Table 1).

It is noteworthy that the interpretation of the results regarding the relative weight of $\alpha\mathcal{C}\lambda_r$ and $\lambda$ is for a positive $\lambda$ (i.e., if $\lambda_d$ dominates over $\lambda_s$). How can this interpretation be altered in a situation where $\lambda$ is negative? Although this has not been directly tested, we do not expect our interpretation to be altered, since whether the model gives more weight to $\lambda$ or $\lambda_r$ does not depend on the sign of $\lambda$. Note also that there is a possibility that the convective "drying" feedback always dominates on the convective "stability" feedback in models, so that $\lambda$ would always be positive. These aspects remain to be investigated.

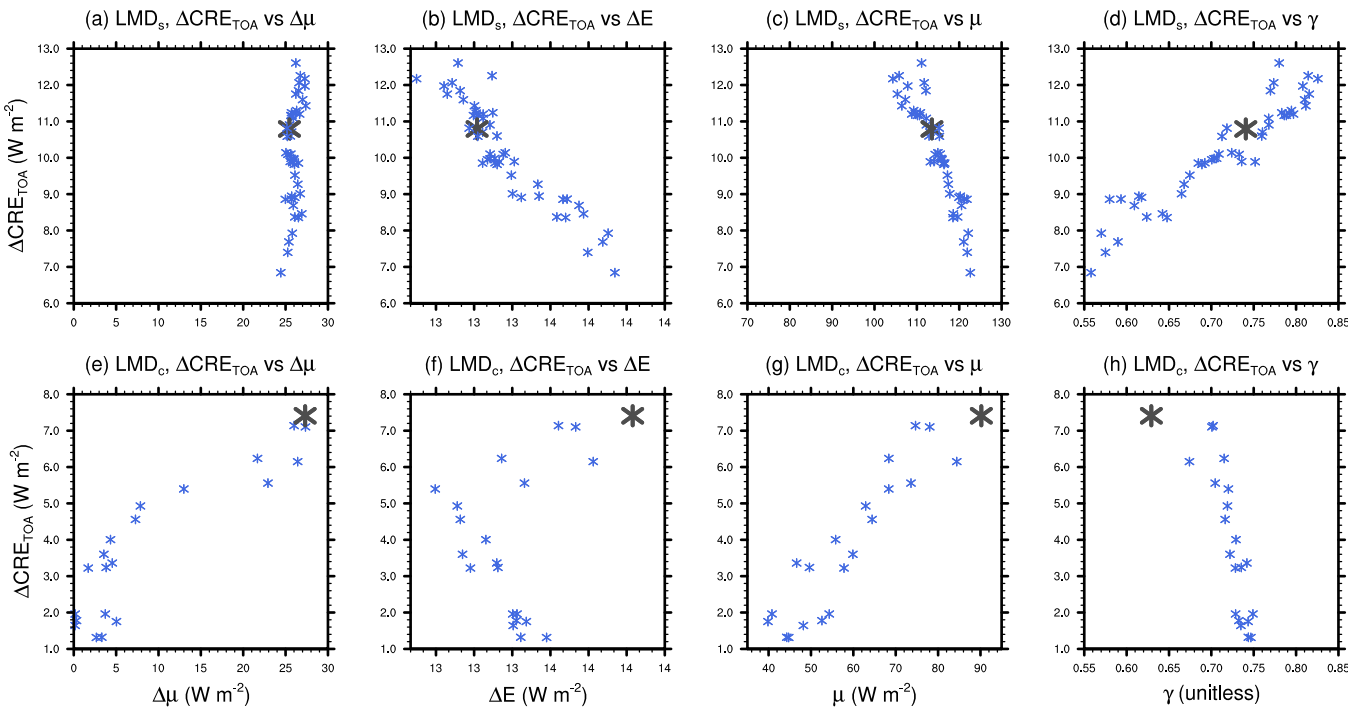


**Figure 6.** Change in top of the atmosphere cloud radiative effects ($\Delta CRE_{TOA}$, in W m$^{-2}$) resulting from an increase in SST of 2 K, as a function of: (from left to right) (a, e) the change in convective mixing ($\Delta\mu$, in W m$^{-2}$), (b, f) the change in latent heat flux ($\Delta E$, in W m$^{-2}$), (c, g) the present-day $\mu$ (in W m$^{-2}$) and (d, h) the present-day shallowness parameter $\gamma$. Results are shown for CRE ON experiments. $LMD_s$ (top row) and $LMD_c$ (bottom row).

## 4. Implication for Low-Cloud Feedbacks

How much can this analysis of the relationship between convective mixing and boundary-layer clouds in a given climate help understand low-level cloud feedbacks as climate is warming? To investigate this issue, we repeat the SCM experiments (section 2.2) by increasing the SST by 2 K (keeping the large-scale subsidence unchanged), and we examine (Figure 6) how the response of TOA cloud radiative effects to warming relates to the changes in convective mixing and latent heat flux and to the convective mixing of the present-day climate. Note that in this study, the term 'cloud feedback' refers to the change in cloud radiative forcing at TOA ($\Delta CRE_{TOA}$) in response to an increased SST, which in the CGILS framework is essentially governed by boundary-layer clouds.

On average, the model predicts a positive low-level cloud feedback in a warmer climate, but its magnitude and how it relates to the changes in convective mixing and latent heat flux strongly depend on the convective scheme. For the control case (when k = 1), a +2K surface warming is associated with a $\Delta CRE_{TOA}$ of about 11 W m$^{-2}$ in $LMD_s$ and 7.5 W m$^{-2}$ in $LMD_c$ (the difference is larger when we activate both convective and nonconvective clouds - not shown). In both cases, however, $\Delta\mu$ and $\Delta E$ are roughly similar ($\sim$ 25 W m$^{-2}$ and 13–14 W m$^{-2}$, respectively). Moreover, when $|\lambda| > |\alpha\mathcal{C}\lambda_r|$ (i.e., $LMD_c$), the low-cloud feedback is stronger when the convective mixing increases more with warming (Figure 6e) and when present-day convective mixing is stronger (Figure 6g). However, when $|\alpha\mathcal{C}\lambda_r| > |\lambda|$ (i.e., $LMD_s$), the low-cloud feedback is enhanced for weaker increase in latent heat flux (Figure 6b) and weaker present-day $\mu$ (Figure 6c).

### 4.1. Applicability of the Framework (Section 3.1)

To understand these two contrasting behaviors, we use equations (3) and (5) and replace the sensitivities to increased $k$ (i.e., the $d$'s) by the responses to increased SST (i.e., $\Delta$'s). This allows us to examine how the present-day relationships between $f$, $\mu$ and $E$ (using the estimated coefficients in Table 1) can predict the changes in $f$ given the simulated changes in $\mu$ and $E$ in the warming climate. Note that in equation (4), which predicts the change in $E$, we incorporate the sensitivity of the increased saturation mixing ratio to temperature (i.e., $+\frac{\partial E}{\partial q_s}\frac{\partial q_s}{\partial SST}dSST$ in equation (4)), which we set to 7%/K (Clausius-Clapeyron). Results (Figure 7) show that differences in cloud changes between the two convective schemes are qualitatively reproduced by equations (3) and (5) (compare the blue markers with the solid and dash blue lines), which suggests that the framework presented in section 3.1 and present-day relationships between convective mixing, latent heat flux and boundary-layer clouds can be used to anticipate, at least qualitatively, the contrasted behaviors of $LMD_s$ and $LMD_c$. More specifically, this framework is useful to explain the dependence of low-level cloud feedbacks to present-day $\mu$ (or $k$), but it cannot be used to reconstruct the absolute value of the feedbacks (or cloud

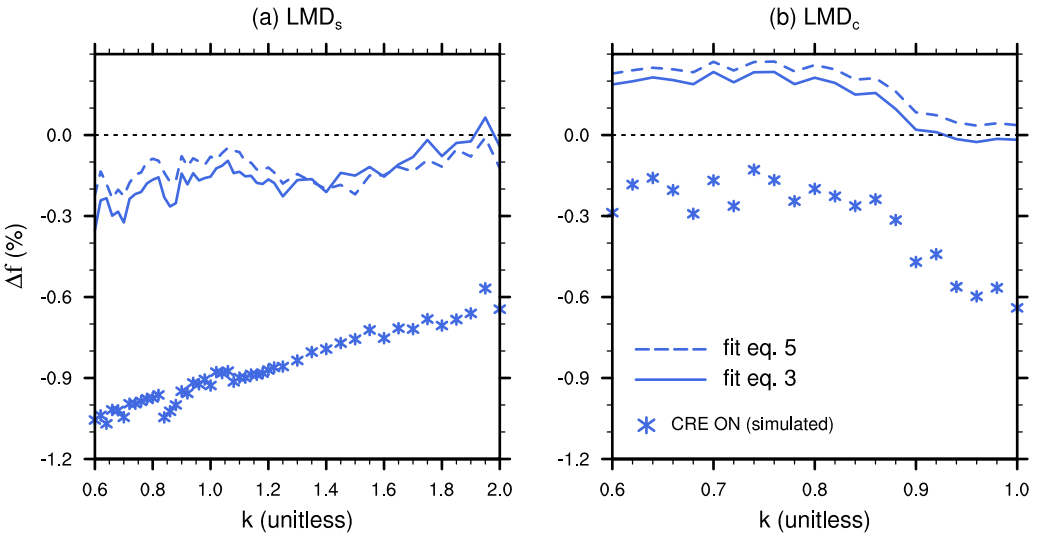


**Figure 7.** Change in boundary-layer cloud fraction ($\Delta f$, in %) as a function of $k$ (markers), resulting from an increase in SST of 2 K, when using (a) $LMD_s$ and (b) $LMD_c$. Solid lines represent multiple least-square regression fits when using the coefficients $\mathcal{C}$ and $\mathcal{T}$ from Table 1 in equation (3) and replacing $d$'s (sensitivities to increased $k$) by $\Delta$'s (responses to increased SST). Dash lines represent the regression fits when using equation (5).

changes), as suggested by the large offset between the simulated and predicted cloud changes in Figure 7. This offset is related to a decrease in the coefficients $\mathcal{C}$ and $\mathcal{T}$ in a warming climate, while their relative contribution to variations in $f$ remains similar (not shown). These changes in $\mathcal{C}$ and $\mathcal{T}$ are likely to be related to the enhanced vertical gradient of MSE between the free troposphere and the boundary-layer in a warmer climate (a consequence of the Clausius-Clapeyron relationship), which yields an increased large-scale vertical advection of MSE and a decreased boundary-layer cloud fraction (not shown–see also *Brient and Bony* [2013]). The offset is at first order independent of $k$ (Figure 7) and therefore probably reflects a shift toward a new climate state, associated to changes in the large-scale environment. Our framework cannot capture this shift in climate state, but the interpretation of cloud responses to changes in smaller-scale processes in a warming climate (i.e., turbulence, convection, radiation)–which is the purpose of our framework - appears to be independent to it.

### 4.2. Interpretation of Low-Level Cloud Changes in a Warming Climate

#### 4.2.1. Dependence on Convective Mixing

The overall differences in low-cloud feedbacks between the two models are explained to a large extent by (i) a stronger sensitivity of boundary-layer clouds to convective mixing ($\mathcal{C}$) in $LMD_s$ compared to $LMD_c$ and (ii) $\Delta\mu$, which is stronger when the present-day convective mixing ($\mu$) is weaker in $LMD_s$ (Figure 8a), while $\Delta\mu$ is stronger when $\mu$ is stronger in $LMD_c$ (Figure 8b). Therefore, and according to the present-day relationship between $f$ and $\mu$, we expect the low-cloud feedback to be stronger for stronger $\Delta\mu$ (everything else being equal), which occurs for weaker present-day $\mu$ when using $LMD_s$ (Figures 7a and 8a) and stronger present-day $\mu$ when using $LMD_c$ (Figures 7b and 8b).

One reason that could explain the differences in $\Delta\mu$ is related to the rate of increase in convective mixing as a function of convective instability, which partly depends on the closure assumption (section 2.3). Using $LMD_s$, the relationship between the convective mass flux at cloud-base and convective instability (i.e., $M_b \propto \sqrt{CAPE}$) implies an increase in $M_b$ in a warmer climate that is inversely proportional to the present-day convective mass flux (i.e., $\frac{\Delta M_b}{\Delta SST} = \frac{1}{2M_b}\frac{\Delta CAPE}{\Delta SST}$, with nearly constant $\Delta CAPE/\Delta SST$ as $k$ is increased - not shown). Given the tight connection between $M_b$ and $\mu$ (Figure 2b), the change in convective mixing ($\Delta\mu$) is expected to be weaker when $\mu$ is stronger in the present-day climate.

In contrast, when using $LMD_c$, the strong relationship between $M_b$ and $E$ (owing to the closure assumption) and the first order dependence of $\Delta E$ on present-day evaporation (through the Clausius-Clapeyron relation) favors greater $\Delta\mu$ in a warmer climate for high present-day $\mu$, especially for $\mu$ greater than 100 W m$^{-2}$ (Figure 8b).

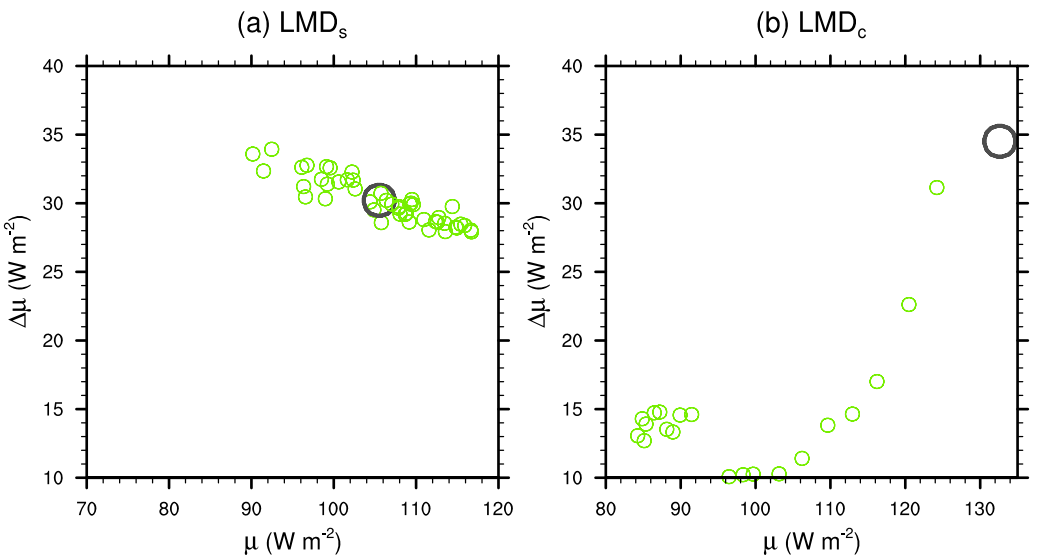


**Figure 8.** Change in $\mu$ ($\Delta\mu$, in W m$^{-2}$), resulting from an increase in SST of 2K as a function of the present-day $\mu$, when using (a) $LMD_s$ and (b) $LMD_c$ in CRE OFF experiments.

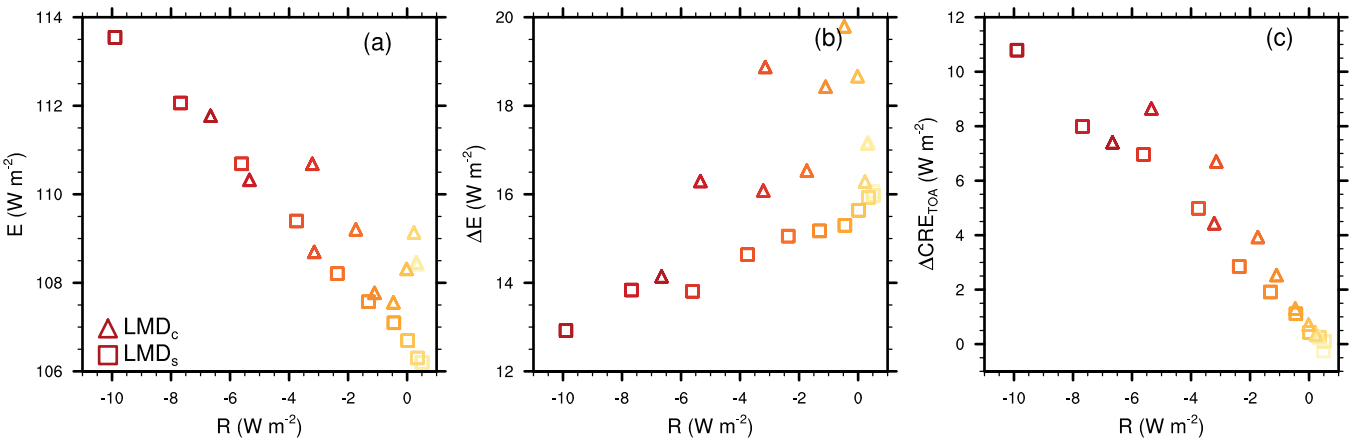


**Figure 9.** Present-day boundary-layer cloud radiative forcing dependence on (a) present-day latent heat flux, (b) change in latent heat flux, and (c) change in boundary-layer cloud radiative forcing - changes result from an increase in SST of 2K. These relationships are based on the $\beta$ experiments (see text), made for $LMD_s$ (empty squares) and $LMD_c$ (empty triangles), in which $\beta$ varies between 0 (CRE OFF) and 1 (CRE ON), from clear to dark brown markers.

#### 4.2.2. Dependence on Present-Day Cloud Radiative Forcing

The contribution of $\mathcal{T}$ to the overall change in boundary-layer cloud fraction (in response to an increased SST) is of second order relative to that of $\mathcal{C}$ (see standardized coefficients in Table 1). Nevertheless, it may become significant when considering the dependence of boundary-layer cloud (changes caused by warming) to present-day convective mixing. When using $LMD_s$, we note from Figure 6b that $\Delta E$ is weaker and $\Delta CRE_{TOA}$ stronger when present-day mixing is weaker. This correlation appears to be related to how the cloud radiative forcing depends on convective mixing in present-day simulations. More specifically, in $LMD_s$, we argue that when low-clouds exert a stronger radiative cooling in the boundary-layer, they influence low-level stability and surface-based turbulence more strongly (i.e., $\alpha\lambda_r$ is stronger). Therefore, as convective mixing strengthens in a warmer climate (Figure 6a), the reduced low-cloud radiative cooling contributes to decrease surface-based turbulence more strongly, thus enhancing more strongly the low-cloud feedback, when the present-day cloud radiative forcing is stronger. This effect can be seen in Figure 7a (by comparing the solid and dashed curves): when using equation (5), both the changes in $f$ and $E$ are predicted given the simulated change in $\mu$ using the constant coefficients in Table 1. Therefore, if the changes in $f$ and $E$ depend on the variation of $\alpha\lambda_r$ with $\mu$, then we expect $\Delta E$ and $\Delta f$ to be less sensitive to $\mu$ (or $k$) when they are predicted using equation (5) (dashed line in Figure 7a) than using equation (3) (solid line in Figure 7a); the difference is stronger for $\Delta E$ (not shown).

To investigate further the dependence of the low-cloud feedback on present-day cloud radiative forcing, we ran additional experiments in which we modulated the contribution of the cloudy component ($R$) in the net atmospheric radiative heating rate ($R_T = R_0 + \beta R$), of the control experiment (when k = 1), by varying $\beta$ between 0 and 1 (Note that $\beta = 0$ in CRE OFF experiment, and $\beta = 1$ in CRE ON experiment), thus making clouds more or less radiatively active, everything else (cloud fraction, vertical distribution, cloud water content) equal. The results, presented in Figure 9a confirm that, as the clouds are more radiatively active in the boundary-layer (i.e., as $\beta$ is increased), the positive feedback between latent heat flux and $R$ in the present-day climate ($\alpha\lambda_r$) is enhanced and the low-cloud feedback ($\Delta CRE_{TOA}$) is enhanced (consistent with the $\beta$-feedback of *Brient and Bony* [2012]): as the surface warms, the increase in E is weakened for stronger $\alpha\lambda_r$ (in particular when using $LMD_s$ - Figure 9b), yielding a stronger low-cloud feedback (Figure 9c).

As a result, since in the present-day climate a stronger $\mu$ means "weaker low-cloud radiative cooling" and thus "weaker $\alpha\lambda_r$", the low-cloud feedback is reduced in a warmer climate. Note, however, that this mechanism is more efficient in models that produce a stronger relationship between latent heat flux and low-cloud radiative cooling ($LMD_s$); in $LMD_c$, E is more strongly related to convective mixing than to cloud radiative cooling, so this effect is less pronounced.

#### 4.2.3. Dependence on Present-Day Cloud Vertical Distribution

As discussed in introduction (section 1), the shallowness of low-clouds is strongly related to the lower-tropospheric convective drying in CMIP5 models, and may exert, for some models, a control on the strength

of the low-cloud feedback (for models having shallower clouds and stronger convective drying in the present-day climate–*Brient et al*. [2016]). How much can the present study help understand the link between the shallowness of low-clouds, convective mixing and low-cloud feedback? To address this question, we examine various relationships (not shown) using the parameter $\gamma$, which represents how bottom-heavy (large $\gamma$) or top-heavy (small $\gamma$) the low-cloud profile is [*Brient et al*., 2016]. According to the definition given by *Brient et al*. [2016], $\gamma = CF_{950}/(CF_{850} + CF_{950})$, where $CF_{950}$ is the averaged cloud fraction between 1000 and 900 hPa, and $CF_{850}$ the averaged cloud fraction between 900 and 800 hPa. As $\mu$ increases, the model dries the lower-troposphere and moistens upper levels (Figures 4a and 4f), and produces deeper clouds with reduced cloud fraction at lowest levels (Figures 4d and 4i), which yields smaller $\gamma$. This mechanism, which has been identified to explain how convective mixing controls the response of low-level clouds to surface warming [*Sherwood et al*., 2014; *Brient et al*., 2016], is at play in the model, but it is more efficient when $|\alpha \mathcal{C} \lambda_r| > |\lambda|$ (i.e., for $LMD_s$). For this model, the stronger $\gamma$ in the present-day climate, the stronger the low-cloud feedback (Figure 6d); this is consistent with the discussion above, since shallower clouds exert a stronger radiative cooling of the boundary-layer and interact more efficiently with $k_0$ (higher $\alpha\lambda_r$). In $LMD_c$, this relationship between $\gamma$ and the low-cloud feedback is not seen (Figure 6h), suggesting that it may work only in models for which $|\alpha \mathcal{C} \lambda_r| > |\lambda|$.

Therefore, these findings support *Brient et al*.'s [2016] results showing that for some models, shallower low-clouds in the present-day climate yield stronger low-cloud feedbacks, although this occurs for weaker present-day convective mixings (Figure 6), rather than stronger mixings as suggested in *Brient et al*. [2016]. Note however that the formulation of the convective drying parameter in *Brient et al*. [2016] implies a strong dependence between convective drying and low-level cloud fraction by construction. We tested their definition of the convective drying parameter, $\epsilon_c$ (not shown), and reached the same conclusion that boundary-layer clouds are shallower (i.e., cloud fraction at lowest levels is stronger) when the convective drying parameter $\epsilon_c$ is stronger.

In this section, we have demonstrated that understanding the present-day relationships between convective mixing, latent heat flux and boundary-layer clouds can be highly valuable to explain the dependance of low-level cloud feedbacks to present-day convective mixing and the constrasted behaviors between the two convective schemes. Most importantly, when present-day low-level clouds exert a stronger radiative cooling of the boundary-layer and interact more strongly with latent heat flux, the overall low-cloud feedback is stronger and strengthens with decreasing present-day $\mu$. However, the convective scheme that favors the coupling between convective mixing and latent heat flux exhibits a weaker low-cloud feedback, which strengthens with increasing present-day convective mixing.

## 5. Conclusion and Discussion

It is well recognized that the boundary-layer cloud fraction is influenced by two basic antagonistic mechanisms: shallow convective mixing, which dries the lower atmosphere, and reduces the low-cloud fraction, and turbulent moistening, which enhances the cloud amount at low levels. In this study, we show (in section 3) that convective mixing, turbulent moistening and cloud radiative forcing are coupled to each other through two additional mechanisms, which can strengthen or damp these two basic processes, and thus modulate the sensitivity in boundary-layer cloud amount to a change in convective mixing. These mechanisms are all at play in the model, but the importance of one mechanism relative to the other depends on the convective scheme, as follows:

1. The sensitivity of latent heat flux to convective mixing strongly depends on the relative impact of the convection scheme on lower-tropospheric stability and drying. In LMDZ, whatever the convective scheme, more weight is given to convective drying than to convective warming, which yields an increase in latent heat flux as convective mixing is enhanced. By increasing latent heat flux, this mechanism damps the decrease in low-cloud fraction initially induced by the convective mixing. Moreover, for a given latent heat flux, the efficiency of the convective mixing at drying at levels of low-level clouds (i.e., $\mathcal{C}$) explains the different sensitivities in boundary-layer cloud fraction to convective mixing between the convection schemes.
2. The relative sensitivity of the latent heat flux to low-cloud radiative cooling and convective mixing is also crucial to explain the different sensitivities in low-level cloud radiative cooling to convective mixing

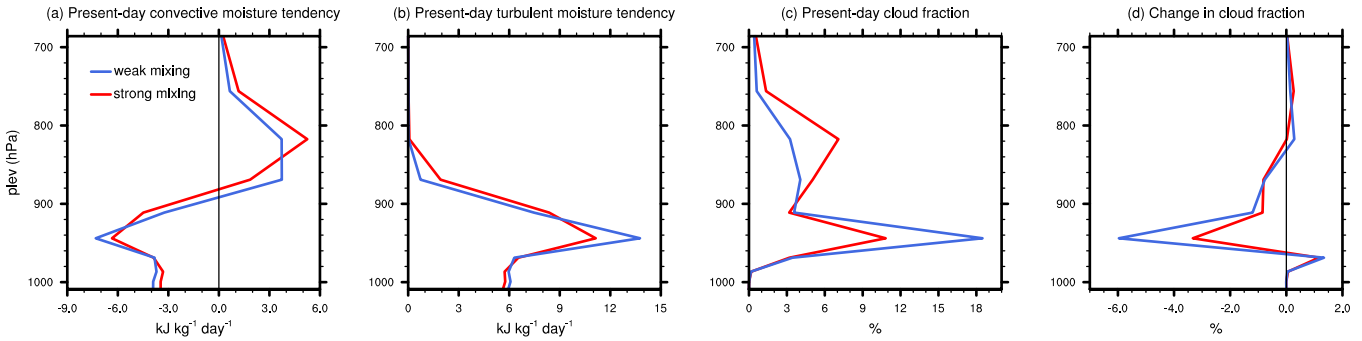


**Figure 10.** Present-day moisture tendency due to (a) convection (in kJ kg$^{-1}$ d$^{-1}$) and (b) turbulence (in kJ kg$^{-1}$ d$^{-1}$), (c) present-day cloud fraction (in %) and (d) change in cloud fraction as a response to increased SST of 2 K (in %) using $LMD_s$ in an aquaplanet configuration. Profiles are shown for two different convective mixing parameters (blue line: strong mixing, red line: weak mixing). Results are shown for the subtropical area (i.e., zonal average at 20°)

between the convection schemes. When more weight is given to the former (i.e., $|\alpha\mathcal{C}\lambda_r| > |\lambda|$), the sensitivity of low-level clouds to convective mixing is enhanced. In contrast, when a convective scheme favors the coupling between latent heat flux and convective mixing (i.e., $|\lambda| > |\alpha\mathcal{C}\lambda_r|$), the sensitivity of low-level cloud is reduced.

3. The relative importance of these two feedback processes depends, to some extent, on the closure hypothesis in the convective scheme: a closure in CAPE gives more weight to $\lambda_r$, while a closure in moisture convergence gives more weight to $\lambda$. It also depends on how radiatively active the clouds are in the present-day climate.

How the low-cloud feedbacks predicted by the models depend on these present-day relationships is addressed in section 4. The efficiency of the convective mixing at reducing boundary-layer cloud fraction ($\mathcal{C}$) along with the actual change convective mixing in a warming climate ($\Delta\mu$, which partly depends on the closure of the convective parametrization) explains to a large extent the overall difference in boundary-layer cloud feedbacks between the two convective schemes. Moreover, the importance that models give to $\alpha\mathcal{C}\lambda_r$ relative to $\lambda$ largely controls the sensitivity of the low-cloud feedbacks to present-day convective mixing, by modulating the increase in latent heat flux in response to increased SST ($\Delta E$). When present-day low-level clouds exert a stronger radiative cooling of the boundary-layer and interact more strongly with latent heat flux (i.e., when $|\alpha\mathcal{C}\lambda_r| > |\lambda|$), the low-cloud feedback weakens with increasing present-day $\mu$ (by reducing the increase in latent heat flux). On the contrary, if $|\lambda| > |\alpha\mathcal{C}\lambda_r|$, the low-cloud feedback tends to be stronger for large present-day convective mixing.

These insights are based on the analysis of SCM simulations and therefore the question arises as to how relevant they are to interpret GCM simulations. We address this question by performing a global GCM experiment using the ISPL-CM5A-LR model ($LMD_s$) in an aquaplanet configuration (for present-day and SST + 4K experiments), by modulating the parameter controling the efficiency of convective precipitation (see Appendix B). Preliminary results (Figure 10 and Table 2) highlight similar features for subtropical regions and at the global scale, as those presented for $LMD_s$ in the SCM configuration:

1. In the present-day climate, increasing convective mixing dries the lower atmosphere, reduces the turbulent flux of moisture and the cloud fraction at low atmospheric levels and yields deeper clouds (Figures 10a–10c).
2. In a warmer climate, the decrease in low-level cloud fraction is stronger when the present-day convective mixing ($\mu$) is weaker and boundary-layer clouds are shallower (Figure 10d and Table 2). This occurs in association with stronger increase in convective mixing and weaker increase in latent heat flux (Table 2).

The mechanisms studied here are therefore robust in 3-D aquaplanet simulations (at least for $LMD_s$). Note also that *Stevens et al.* [2016] found similar relationships between convective mixing and boundary-layer clouds in the ECHAM6 atmospheric GCM. However, unlike in the SCM configuration, increased mixing seems also to be associated with an upward shift of the lower-tropospheric convective drying (Figure 10a) and turbulent moistening (Figure 10b), which results in an increased latent heat flux with $\mu$ (Table 2).

**Table 2.** Present-Day and +2K SST-Induced Changes in Latent Heat Flux (in W $m^{-2}$), Boundary-Layer Cloud Fraction (in %) and Convective Mixing (in W $m^{-2}$) in Subtropical Regions (i.e., Zonal Average at 20°) and for Global Averages (into Brackets) for the IPSL-CM5A-LR Model in an Aquaplanet Configuration

| | Present-Day | | +2K SST-Induced Change | |
|---|---|---|---|---|
| $\Delta p_c$ | 10 mb | 150 mb | 10 mb | 150 mb |
| $\mu$ | 53.7 (78.0) | 66.1 (82.0) | 15.5 (9.1) | 12.5 (8.4) |
| $LH$ | 116.9 (109.2) | 118.4 (110.9) | 12.2 (7.9) | 13.4 (8.6) |
| $f$ | 31.0 (24.5) | 27.8 (22.9) | −5.9 (−4.3) | −3.5 (−2.9) |

*Sherwood et al*. [2014] and *Brient and Bony* [2013] showed that the large-scale component of the lower-tropospheric mixing also plays an important role in low-cloud feedbacks through the vertical transport of MSE between the boundary-layer and the free troposphere. Therefore, while these experiments confirm the relevance of SCM experiments to understand boundary-layer cloud feedbacks in a 3-D framework, they also stress the need to deepen our understanding of the role of the large-scale circulation in the relationship between latent heat flux, convective mixing and boundary-layer clouds in GCMs.

We have demonstrated that the coupling between convective mixing and low-clouds, which affects the strength of low-cloud feedbacks, depends on convective scheme. It implies that the inter-model spread in low-cloud feedbacks also presumably depends, to some extent, on convective schemes. Nevertheless, given the importance of the coupling between convective mixing and turbulent flux of moisture, the relationship between convective mixing and low-clouds (and thus the strength of low-cloud feedbacks) also depends on the turbulence parameterization. This idea is supported by recent findings in *Webb et al*. [2015], who showed that the inter-model spread of low-cloud feedbacks is not reduced when the convective parameterizations are switched off.

The insights gained from this study about the physical processes that control marine low-clouds in climate models, and their dependence on the representation of convective processes, allows us to refine some of the strategies recently proposed to constrain the strength of low-cloud feedbacks [e.g., *Sherwood et al*., 2014; *Brient et al*., 2016]. Our study shows that the strength of the lower-tropospheric convective mixing constitutes a key controlling factor of the strength of low-cloud feedbacks in models. However, it makes it clear that this control *closely depends on how convective mixing couples to surface turbulent fluxes and boundary-layer cloud-radiative effects*. Therefore, evaluating the strength of the model convective mixing alone is unlikely to be sufficient to constrain the strength of cloud feedbacks. The same thing applies to the shape of the vertical distribution of low-level clouds that was found to modulate the strength of the low-cloud feedback but in a way that depends on other factors (Figures 6d and 6h). What this study suggests, on the other hand, is that evaluating *the relationship between lower-tropospheric convective mixing, surface latent heat flux and shallow cumulus clouds* in models will be a more effective strategy to constrain the strength of low-cloud feedbacks. For instance, it could help determine whether the models predicting $|\propto C\lambda_r| > |\lambda|$ (and thus a stronger low-cloud feedback), are more or less credible than those predicting the opposite.

Such relationships could be first evaluated using LES simulations such as those performed as part of CGILS [*Blossey et al*., 2013] or in connection to the BOMEX or RICO campaigns [*Siebesma et al*., 2003; *Rieck et al*., 2012; *Seifert and Heus*, 2013]. However, nothing would be more powerful than constraining these relationships using observations. Data from cloud observatories in regions of shallow cumulus regimes could be very valuable for this purpose [e.g., *Nuijens et al*., 2014; *Stevens et al*., 2016]. However, given recent advances in our understanding of low-cloud feedbacks, time is ripe for organizing a field campaign especially designed to elucidate the interplay between shallow cumulus clouds, lower-tropospheric convective mixing, surface turbulent fluxes, radiative processes and large-scale environmental factors [*Bony and Stevens*, 2016]. Such a campaign would offer a great opportunity to constrain, finally, the strength of low-cloud feedbacks and thus to reduce, hopefully, the long-standing uncertainty in climate sensitivity.

## Appendix A: Extended Model Description

We provide here an extended description of the physical parameterizations used in the IPSL-CM5A-LR SCM, which are relevant for the representation of boundary-layer clouds. These include the turbulent diffusion, convection and cloud schemes.

Turbulent transport in the planetary boundary layer is treated as a vertical diffusion with an eddy diffusion coefficient depending on the local stability (through the Richardson number) and on the mixing length

[*Laval et al.*, 1981]. Up-gradient transport of heat in stable regions is ensured by adding a counter-gradient of −1 K/km to the vertical derivative of potential temperature [*Deardorff*, 1966].

The model is run with two different convection schemes: the *Emanuel convection scheme* ($LMD_s$) and the *Tiedtke convection scheme* ($LMD_c$).

The Emanuel scheme is based on a mass flux representation of adiabatic saturated updraughts and downdraughts, unsaturated downdraughts (driven by reevaporation of precipitation) and the induced motions of the environmental air. The lateral mixing between cloud and environmental air is based on the "episodic mixing and buoyancy sorting" scheme developed by *Emanuel* [1991]. Triggering and closure depend on tropospheric stability (CAPE) and convection inhibition (CIN).

The *Tiedtke* [1989] scheme parametrizes convective mass fluxes as one convective cloud, which is represented as one single saturated updraught plus one single saturated downdraught. The lateral mixing between the cloud and the environment is assumed to occur through turbulent exchange at cloud edge, at a rate that is prescribed and specified for each type of convection (i.e., shallow, middle and deep), and through organized inflow and outflow associated with large-scale moisture convergence. Triggering depends on tropospheric stability, while closure relies on moisture and temperature convergence from surface turbulent fluxes and the large-scale circulation.

The statistical cloud scheme describes the subgrid-scale variability of total water within each gridbox by a generalized log-normal distribution of total water content with zero at lower bound (positively skewed–*Bony and Emanuel* [2001]). Nonconvective cloud fraction and cloud water content are diagnosed from the large-scale value of total water and humidity at saturation predicted by the model, and by parameterizing the width of the distribution as a function of the vertical profile of large-scale total water [*Bony and Emanuel*, 2001; *Hourdin et al.*, 2006]. Nonconvective clouds are predicted in the same way whatever the convective scheme used.

The parametrization of clouds associated with cumulus convection depends on the convective scheme used in the model. When using $LMD_s$, the cloud fraction is diagnosed from the profile of in-cloud water content predicted by the convective scheme, and from the large-scale degree of saturation of the atmosphere [*Bony and Emanuel*, 2001]. When using $LMD_c$, an homogeneous cloud fraction from cloud base to cloud top is assumed, whose value at each level is a function of the vertically integrated moistening tendency due to convection [*Hourdin et al.*, 2006].

The results presented here are qualitatively similar when activating both convective and nonconvective cloud schemes or nonconvective clouds alone.

## Appendix B: Additional Parameter-Perturbed Experiments

When using $LMD_s$ (in single-column and aquaplanet configurations), an additional set of experiments consists in modulating the efficiency of convective precipitation, which is a tunable parameter of the model. More specifically, this parameter is defined as a critical cloud depth below which no precipitation occurs (denoted as $\Delta p_c$). Increasing this parameter induces deeper nonprecipitating clouds, thus yielding a decreased efficiency of convective precipitation. In the model, the default value for this parameter is $\Delta p_c = 150$ mb. For the SCM experiments, we have explored the range from 10 to 180 mb (results are similar to the *k*-experiments and are not shown). For the aquaplanet experiments, we have compared model results for $\Delta p_c = 10$ mb (weak mixing) and $\Delta p_c = 150$ mb (strong mixing); preliminary results are presented in section 5.

## Appendix C: Estimates of $\mathcal{C}$, $\mathcal{T}$, $\lambda$ and $\lambda_r$

We derive estimates of $\mathcal{C}$, $\mathcal{T}$, $\lambda$ and $\lambda_r$ through multiple least-squares regression fits in CRE ON and CRE OFF experiments, where (i) $\mathcal{C}$ and $\mathcal{T}$ are the partial coefficients from regression of $df$ against $d\mu$ and $dE$ (equation (3)), and (ii) $\lambda$ and $\lambda_r$ the coefficients from regression of $dE$ against $d\mu$ and $dR$ (equation (4); note that for CRE OFF experiments, $\lambda$ is estimated through simple regression of $dE$ against $d\mu$).

The change in the variable $x$ (where $x$ refers to $f$, $\mu$, $dE$ or $dR$) as the sensitivity parameter $k$ is increased is given by:

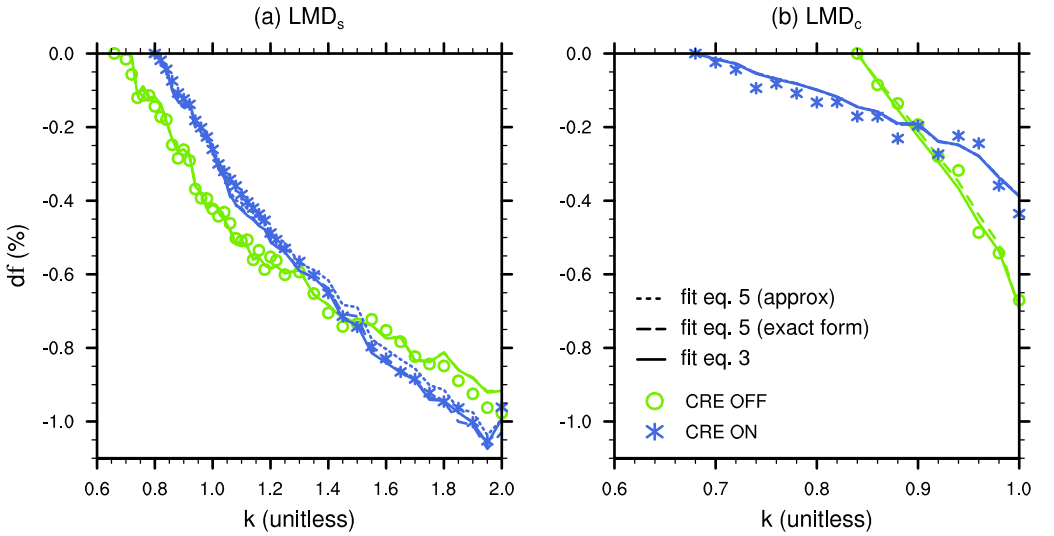


**Figure C1.** Variation in boundary-layer cloud fraction (*df*, in %) as a function of *k* (markers) for (a) $LMD_s$ and (b) $LMD_c$. The code for markers' colors is the same as for Figure 5. Lines represent multiple least-square regression fits when using coefficients from Table 1 in equation (3) (solid) and equation (5) in its exact form (dash) and approximate form (dotted).

$$dx(k) = x(k_{\min}) - x(k) \tag{C1}$$

In order to minimize the error in the fits, regressions are applied to the *most* linear part of the data points (cf. Figure 5), which depends on the model and whether clouds are radiatively active or not. Figure C1 shows that both equations (3) and (5) (in its exact or approximate form) with coefficients from Table 1 are able to predict the variations in boundary-layer cloud fraction as *k* is increased over the selected ranges of data points.

To compare the relative contribution of $d\mu$ and $dE$ (in equation (3)) and $d\mu$ and $dR$ (in equation (4)) in the variations of $f$ and $E$, respectively, we computed the standardized regression coefficients (normalized by standard deviations). For instance, the standardized coefficient $\mathcal{C}$ is given by $\mathcal{C}\frac{\sigma_{d\mu}}{\sigma_{df}}$, where $\sigma_{d\mu}$ and $\sigma_{df}$ are the standard deviations of $d\mu$ and $df$, respectively.

**Acknowledgments**
This work was supported by a postodctoral research grant funded by CNES (Centre National d'Études spatiales), the Labex L-IPSL (grant ANR-10-LABX-0018), the European Research Council (ERC) grant 694768, and the project LEFE/MEDEE from INSU (Institut national des sciences de l'Univers). We thank Ionela Musat for producing the aquaplanet model output, Florent Brient for providing support with the CGILS setup and Nicolas Rochetin for useful discussions. Thanks to the three reviewers for their constructive comments and helpful suggestions on an earlier version of the manuscript. Data and source codes that were used to generate the results may be obtained from the authors (email: jessica.vial@lmd.jussieu.fr).

## References

Blossey, P. N., et al. (2013), Marine low cloud sensitivity to an idealized climate change: The CGILS LES intercomparison, *J. Adv. Model. Earth Syst.*, *5*, 234–258, doi:10.1002/jame.20025.

Bony, S., and J.-L. Dufresne (2005), Marine boundary layer clouds at the heart of tropical cloud feedback uncertainties in climate models, *Geophys. Res. Lett.*, *32*, L20806, doi:10.1029/2005GL023851.

Bony, S., and K. A. Emanuel (2001), A parameterization of the cloudiness associated with cumulus convection; evaluation using TOGA COARE data, *J. Atmos. Sci.*, *58*(21), 3158–3183, doi:10.1175/1520-0469(2001)058¡3158:APOTCA¿2.0.CO;2.

Bony, S., and B. Stevens (2016), EUREC$^4$A, the field study: A draft white paper.

Bony, S., J.-L. Dufresne, H. Le Treut, J.-J. Morcrette, and C. Senior (2004), On dynamic and thermodynamic components of cloud changes, *Clim. Dyn.*, *22*(2-3), 71–86, doi:10.1007/s00382-003-0369-6.

Bretherton, C. S. (2015), Insights into low-latitude cloud feedbacks from high-resolution models, *Philos. Trans. R. Soc. A*, *373*(2054), 20140415.

Bretherton, C. S., P. N. Blossey, and C. R. Jones (2013), Mechanisms of marine low cloud sensitivity to idealized climate perturbations: A single-LES exploration extending the CGILS cases, *J. Adv. Model. Earth Syst.*, *5*, 316–337, doi:10.1002/jame.20019.

Brient, F., and S. Bony (2012), How may low-cloud radiative properties simulated in the current climate influence low-cloud feedbacks under global warming?, *Geophys. Res. Lett.*, *39*, L20807, doi:10.1029/2012GL053265.

Brient, F., and S. Bony (2013), Interpretation of the positive low-cloud feedback predicted by a climate model under global warming, *Clim. Dyn.*, *40*(9-10), 2415–2431, doi:10.1007/s00382-011-1279-7.

Brient, F., T. Schneider, Z. Tan, and S. Bony (2016), Shallowness of tropical low clouds as a predictor of climate models' response to warming, *Clim. Dyn.*, *47*(433).

Charney, J., A. Arakawa, D. J. Baker, B. Bolin, R. E. Dickinson, R. M. Goody, C. E. Leith, H. M. Stommel, and C. I. Wunsch (1979), Carbon dioxide and climate: A scientific assessment, technical report, MIT Press.

Deardorff, J. W. (1966), The counter-gradient heat flux in the lower atmosphere and in the laboratory, *J. Atmos. Sci.*, *23*(5), 503–506.

Dee, D. P., et al. (2011), The ERA-Interim reanalysis: Configuration and performance of the data assimilation system, *Q. J. R. Meteorol. Soc.*, *137*(656), 553–597, doi:10.1002/qj.828.

Dufresne, J.-L., et al. (2013), Climate change projections using the ipsl-cm5 earth system model: From cmip3 to cmip5, *Clim. Dyn.*, *40*(9-10), 2123–2165.

Emanuel, K. A. (1991), A scheme for representing cumulus convection in large-scale models, *J. Atmos. Sci.*, *48*(21), 2313–2329.
Emanuel, K. A. (1993), A cumulus representation based on the episodic mixing model: The importance of mixing and microphysics in predicting humidity, *AMS Meteorol. Monogr.*, *24*(46), 185–192.
Fasullo, J. T., and K. E. Trenberth (2012), A less cloudy future: The role of subtropical subsidence in climate sensitivity, *Science*, *338*(6108), 792–4, doi:10.1126/science.1227465.
Fermepin, S., and S. Bony (2014), Influence of low-cloud radiative effects on tropical circulation and precipitation, *J. Adv. Model. Earth Syst.*, *6*, 513–526, doi:10.1002/2013MS000288.
Gettelman, A., J. Kay, and K. Shell (2012), The evolution of climate sensitivity and climate feedbacks in the community atmosphere model, *J. Clim.*, *25*(5), 1453–1469.
Grandpeix, J.-Y., V. Phillips, and R. Tailleux (2004), Improved mixing representation in Emanuel's convection scheme, *Q. J. R. Meteorol. Soc.*, *130*(604), 3207–3222, doi:10.1256/qj.03.144.
Hourdin, F., et al. (2006), The LMDZ4 general circulation model: Climate performance and sensitivity to parametrized physics with emphasis on tropical convection, *Clim. Dyn.*, *27*(7-8), 787–813, doi:10.1007/s00382-006-0158-0.
IPCC (2013), Summary for Policymakers, in *Climate Change 2013: The Physical Science Basis. Contribution of Working Group I to the Fifth Assessment Report of the Intergovernmental Panel on Climate Change*, edited by P. Stocker et al., chap. SPM, pp. 1–30, Cambridge Univ. Press, Cambridge, U. K., doi:10.1017/CBO9781107415324.
Kamae, H., Y., M. Shiogama, T. Watanabe, T. Ogura, T. Yokohata, and M. Kimoto (2016), Lower tropospheric mixing as a constraint on cloud feedback in a multi-parameter multi-physics ensemble, *J. Clim.*, *29*(17), 6259–6275, doi:10.1175/JCLI-D-16-0042.1.
Lamer, K., P. Kollias, and L. Nuijens (2015), Observations of the variability of shallow trade wind cumulus cloudiness and mass flux, *J. Geophys. Res. Atmos.*, *120*, 6161–6178, *doi*:10.1002/2014JD022950.
Laval, K., R. Sadourny, and Y. Serafini (1981), Land surface processes in a simplified general circulation model, *Geophys. Astrophys. Fluid Dyn.*, *17*(1), 129–150.
Masunaga, H., and Z. J. Luo (2016), Convective and large-scale mass flux profiles over tropical oceans determined from synergistic analysis of a suite of satellite observations, *J. Geophys. Res. Atmos.*, *121*, 7958–7974, doi:10.1002/2016JD024753.
Mlawer, E. J., S. J. Taubman, P. D. Brown, M. J. Iacono, and S. A. Clough (1997), Radiative transfer for inhomogeneous atmospheres: RRTM, a validated correlated-k model for the longwave, *J. Geophys. Res.*, *102*(D14), 16,663–16,682.
Nuijens, L., I. Serikov, L. Hirsch, K. Lonitz, and B. Stevens (2014), The distribution and variability of low-level cloud in the North Atlantic trades, *Q. J. R. Meteorol. Soc.*, *140*(684), 2364–2374.
Randall, D. A., et al. (2007), Climate models and their evaluation, in *Climate Change 2007: The physical science basis, Contribution of Working Group I to the Fourth Assessment Report of the IPCC (FAR)*, pp. 589–662, Cambridge Univ. Press.
Rieck, M., L. Nuijens, and B. Stevens (2012), Marine boundary layer cloud feedbacks in a constant relative humidity atmosphere, *J. Atmos. Sci.*, *69*(8), 2538–2550, doi:10.1175/JAS-D-11-0203.1.
Seifert, A., and T. Heus (2013), Large-eddy simulation of organized precipitating trade wind cumulus clouds, *Atmos. Chem. Phys.*, *13*, 5631–5645.
Sherwood, S. C., S. Bony, and J.-L. Dufresne (2014), Spread in model climate sensitivity traced to atmospheric convective mixing, *Nature*, *505*(7481), 37–42, doi:10.1038/nature12829.
Siebesma, A. P., et al. (2003), A large eddy simulation intercomparison study of shallow cumulus convection, *J. Atmos. Sci.*, *60*(10), 1201–1219.
Stevens, B. (2007), On the growth of layers of nonprecipitating cumulus convection, *J. Atmos. Sci.*, *64*(8), 2916–2931.
Stevens, B., S. Bony, and M. Webb (2012), Clouds on-off klimate intercomparison experiment (cookie), European Union Cloud Intercomparison, Process Study and Evaluation (EUCLIPSE) Project.
Stevens, B., et al. (2016), The Barbados cloud observatory-anchoring investigations of clouds and circulation on the edge of the ITCZ, *Bull. Am. Meteorol. Soc.*, 787–801, doi:10.1175/BAMS-D-14-00247.1.
Tiedtke, M. (1989), A comprehensive mass flux scheme for cumulus parameterization in large-scale models, *Mon. Weather Rev.*, *117*(8), 1779–1800, doi:10.1175/1520-0493(1989)117<1779:ACMFSF>2.0.CO;2.
Tomassini, L., A. Voigt, and B. Stevens (2014), On the connection between tropical circulation, convective mixing, and climate sensitivity, *Q. J. R. Meteorol. Soc.*, *141*(689), 1404–1416, doi:10.1002/qj.2450.
Vial, J., J. L. Dufresne, and S. Bony (2013), On the interpretation of inter-model spread in CMIP5 climate sensitivity estimates, *Clim. Dyn.*, *41*(11-12), 3339–3362.
Webb, M. J., and A. P. Lock (2013), Coupling between subtropical cloud feedback and the local hydrological cycle in a climate model, *Clim. Dyn.*, *41*, 1923–1939, doi:10.1007/s00382-012-1608-5.
Webb, M. J., et al. (2006), On the contribution of local feedback mechanisms to the range of climate sensitivity in two GCM ensembles, *Clim. Dyn.*, *27*(1), 17–38, doi:10.1007/s00382-006-0111-2.
Webb, M. J., et al. (2015), The impact of parametrized convection on cloud feedback, *Philos. Trans. R. Soc. A.*, *373*(2054), 20140414.
Wyant, M. C., C. S. Bretherton, and P. N. Blossey (2009), Subtropical low cloud response to a warmer climate in a superparameterized climate model. Part I: Regime sorting and physical mechanisms, *J. Adv. Model. Earth Syst.*, *1*, 7, doi:10.3894/JAMES.2009.1.7.
Yanai, M., S. Esbensen, and J.-H. Chu (1973), Determination of bulk properties of tropical cloud clusters from large-scale heat and moisture budgets, *J. Atmos. Sci.*, *30*, 611–627.
Zelinka, M. D., S. a. Klein, K. E. Taylor, T. Andrews, M. J. Webb, J. M. Gregory, and P. M. Forster (2013), Contributions of different cloud types to feedbacks and rapid adjustments in CMIP5, *J. Clim.*, *26*(14), 5007–5027, doi:10.1175/JCLI-D-12-00555.1.
Zhang, M., C. S. Bretherton, P. N. Blossey, S. Bony, F. Brient, and J.-C. Golaz (2012), The CGILS experimental design to investigate low cloud feedbacks in general circulation models by using single-column and large-eddy simulation models, *J. Adv. Model. Earth Syst.*, *4*, M12001, doi:10.1029/2012MS000182.
Zhang, M., et al. (2013), CGILS: Results from the first phase of an international project to understand the physical mechanisms of low cloud feedbacks in single column models, *J. Adv. Model. Earth Syst.*, *5*, 826–842, doi:10.1002/2013MS000246.